HEDL-TME 77-12
UC-20

MAGNETIC FUSION ENERGY

PROGRESS REPORT

JULY-DECEMBER 1976

HANFORD ENGINEERING DEVELOPMENT LABORATORY
Operated by Westinghouse Hanford Company
A Subsidiary of Westinghouse Electric Corporation

P.O. Box 1970 Richland, WA 99352

Prepared for the U.S. Energy Research and Development Administration under Contract No. EY-76-C-14-2170

NOTICE

Printed in the United States of America
Available from
National Technical Information Service
U.S. Department of Commerce
5285 Port Royal Road
Springfield, Virginia 22161
Price: Printed Copy $5.00 ; Microfiche ~~$2.25~~ $3.00

HEDL-TME 77-12
UC-20

MAGNETIC FUSION ENERGY

PROGRESS REPORT

JULY-DECEMBER 1976

Compiled
by

D. G. Doran

April 1977

Hanford Engineering Development Laboratory

Operated by the **Westinghouse Hanford Company**

A Subsidiary of Westinghouse Electric Corporation

for the United States Energy Research and Development Administration Contract No. EY-76-C-14-2170

HEDL-TME 77-12
UC-20

MAGNETIC FUSION ENERGY

PROGRESS REPORT

JULY-DECEMBER 1976

Compiled by

D. G. Doran

ABSTRACT

This report describes progress in three HEDL programs supported by ERDA's Division of Magnetic Fusion Energy.

Included under the Irradiation Effects Analysis program are (1) some results of computer simulations of low energy displacement events in the 25 to 200 eV range in a lattice representing copper; (2) a brief discussion of a new code (SCAS) for simulating short term annealing of cascades; (3) a discussion of the status and techniques of radiation damage analysis as applied to fusion reactor first walls; and (4) a brief description of the organization of new DMFE task group on Damage Analysis and Fundamental Studies.

The first irradiation test of a torsional creep testing machine is described under the Mechanical Performance of MFE Materials program. A specimen of 20% cold worked stainless steel was irradiated with 15 MeV protons at ~400°C. Significant irradiation-induced creep rates were observed.

In the first report of a new program on Preparation and Presentation of Design Data, it is noted that the scope of the Nuclear Systems Materials Handbook has been expanded to address the needs of current and future MFE programs; copies of the Handbook were provided to organizations participating in near term MFE projects.

CONTENTS

TABLES

FIGURES

FOREWORD

This report describes progress in HEDL and some related offsite programs supported by the Division of Magnetic Fusion Energy of the Energy Research and Development Administration. These programs are:

- Irradiation Effects Analysis
- Mechanical Performance of MFE Materials
- Preparation and Presentation of Design Data.

Previous reports issued in this series are:

HEDL-TME 74-64, December 1974
HEDL-TME 75-24, February 1975
HEDL-TME 75-56, May 1975
HEDL-TME 75-90, July 1975
HEDL-TME-76-7, March 1976
HEDL-TME 76-83, September 1976.

IRRADIATION EFFECTS ANALYSIS (ED-02-03 EDA)

IRRADIATION EFFECTS ANALYSIS

I. OBJECTIVE

The objective of this program is to establish a basis for predicting bulk materials performance under fusion reactor conditions from radiation effects data obtained with fission reactor neutrons, accelerator-based high energy neutrons, and with charged particles.

II. SUMMARY

The atomic motion in a copper lattice following the production of primary knock-on atoms (PKAs) with energies from 25 to 200 eV has been simulated. A mixed Moliére-Englert pair potential was used to model the copper lattice. The computer code COMENT, which employs the dynamical method, was used to analyze the motion of up to 6000 atoms per time step during cascade evolution. The atoms were specified as initially at rest on the sites of an ideal lattice. A matrix of 12 PKA directions and 6 PKA energies was investigated. Displacement thresholds in the <110> and <100> were calculated to be approximately 17 and 20 eV, respectively. A table showing the stability of isolated Frenkel pairs with different vacancy and interstitial orientations and separations is presented. The numbers of Frenkel pairs and atomic replacements are tabulated as a function of PKA direction for each energy. For PKA energies of 25, 50, 75, 100, 150, and 200 eV, the average number of Frenkel pairs per PKA are 0.4, .6, 1.0, 1.2, 1.4, and 2.2 and the average numbers of replacements per PKA are 2.4, 4.0, 3.3, 4.9, 9.3, and 15.8.

A simplified random walk annealing code, SCAS (Stochastic Cascade Annealing Simulator) has been completed for application to the short-term annealing of displacement cascades.

The status of radiation damage analysis as applied to fusion reactor first walls is discussed and assessed. The need for increased understanding of damage production and evaluation is illustrated with a speculative discussion of the role of helium in the nucleation and growth of damage microstructures. The use of semi-empirical damage correlation procedures is also discussed; it is pointed out that such correlations must be guided by knowledge of damage mechanisms because of the necessary extrapolations from test conditions to fusion reactor conditions. It is also pointed out that increased effort is needed in relating irradiation induced microstructural changes to mechanical property changes. This is particularly true because the small available test volumes permit the acquisition of much more microstructural data than mechanical property data.

An ERDA-DMFE task group has been established in the area of Damage Analysis and Fundamental Studies. Its membership, organization, and initial schedule are given.

III. ACCOMPLISHMENTS AND STATUS

COMPUTER SIMULATIONS OF LOW ENERGY DISPLACEMENT CASCADES IN A FACE CENTERED CUBIC LATTICE

J. O. Schiffgens and R. D. Bourquin/W. M. McElroy (HEDL)

A. INTRODUCTION

When a solid is irradiated the effects which result depend on such factors as the nature of the chemical bond which characterizes the solid, the irradiation temperature, and the type and energy of the incident radiation. Radiation transfers momentum directly to a number of atoms referred to as primary knock-on atoms or PKAs. A PKA, once formed, interacts with surrounding lattice atoms initiating a cascade of colliding atoms. Provided a PKA has sufficient energy, some atoms in the cascade are permanently displaced from their lattice sites. The number and spatial distribution of these lattice defects

and the extent to which clusters of them form during cascade evolution are of prime importance for the correlation of irradiation data and the analysis of radiation effects. The processes following the formation of a PKA may be viewed as taking place in three distinct phases: "expansion", "collapse", and "short-term annealing".

The cascade expansion phase extends from the formation of a PKA to that point in time when the energy of the most energetic atom in the cascade falls below the threshold energy required to produce a permanent displacement in an otherwise undisturbed lattice. Depending on the energy of the primary this phase may span 10^{-14} to 10^{-13} seconds. In general, however, lattice atoms surrounding displaced atoms in the cascade are involved in numerous subthreshold encounters, resulting in a much disturbed region of lattice. The subsequent rearrangement of atoms in the disturbed region constitutes cascade collapse.

The cascade collapse phase lasts from the end of cascade expansion until sufficient order is restored to distinguish distinct and stable vacancies, interstitials and clusters of each throughout the cascade region. The significance of this phase is that, except for the sum of the formation energies of the eventually stable defects, the energy deposited by the radiation is spent causing thermal agitation of atoms as the energy flows out from the core of the cascade to the surrounding lattice. A period of 10^{-13} to 10^{-12} seconds is required to allow for sufficient re-establishment of local order that classical diffusion processes may begin.

Once local order is restored, the further rearrangement of atoms involves classical activation processes. This marks the onset of the short-term annealing phase. During this phase, irradiation produced clusters either decay or grow as vacancies and interstitials are absorbed at extended defects, annihilate or cluster. The duration of this phase is a function of temperature and defect density. The

subject of short-term annealing has been discussed elsewhere[1] and will not be taken up here.

B. PROCEDURE

Due to the relative ease of analyzing binary collisions there is a strong tendency to want to treat the evolving cascade as a series of binary collisions. Although this approach appears attractive at high energies it is surely a poor approximation at low energies where many-body considerations are important. This report describes work in which the dynamical method is employed for the analysis of processes occurring in phases one and two of cascade evolution. In many respects, the work reported here complements and extends the early work of Gibson et al.[2]

Although the computer code used in this study, COMENT, was written specifically for the analysis of isolated and interacting cyrstal defects, the code is quite versatile and may readily be used to analyze the dynamics of cascade evolution. COMENT employs the dynamical method, according to which the motion of N atoms, each of mass m, is treated by setting up and simultaneously solving the corresponding 3N classical equations of motion which are coupled through a two-body interatomic potential function. The equations are integrated by substitution of a central finite difference to yield the trajectories and velocities of all atoms as a function of time. Since this analysis concerns both calculations on the stability of various static equilibrium configurations of a vacancy and an interstitial, and calculations on the dynamics of cascade evolution, COMENT is run in two modes. When analyzing displacement cascades the time step is chosen and the code is operated so as to rigorously conserve energy. When analyzing static equilibrium configurations of a vacancy and an interstitial, strict conservation of energy is not necessary so the time step is lengthened and the velocity components of each atom are set to zero each time step. Detailed descriptions of COMENT are presented elsewhere.[3,4]

No attempt was made in this study to compare results from calculations with different potentials. Rather, all calculations reported here were performed with a mixed Moliére-Englert pair potential. Because a large amount of information is available on binary collision simulations for copper using the Moliére approximation to the Thomas Fermi screening function[5,6], this function was used to describe the short range nuclear repulsion part of the interatomic potential. The Moliére approximation has the form

$$\phi(r) = \frac{Z_1 Z_2 e^2}{r} f(r) \qquad r \leq 1.55\text{Å} \qquad (1)$$

with

$$f(r) = .25 \exp(-.3r/a) + .55 \exp(-1.2r/a) + .10 \exp(-6.0r/a) \qquad (2)$$

where Z_1 e and Z_2 e are the nuclear charges of the colliding atoms and a is the screening radius. Torrens and Robinson[5] chose a value of .0738Å for a so that the Moliére potential would have the same value at the nearest neighbor distance in the crystal as a Born-Mayer potential whose parameters were determined from elastic constant data. It so happens that this screening radius in the mixed Moliére-Englert pair potential described here yields calculated <100> (89°, 1°) and <110> (89°, 44°) displacement thresholds of approximately 20 and 17 eV, respectively, in reasonable agreement with the <100> and <110> threshold energies reported by Jung et al.[7] Hence, the value .0738Å was used in this work.

In order to satisfactorily simulate thermodynamic behavior and obtain the correct elastic constant data for the lattice, the Englert[8] function was used to describe the long range part of the interatomic potential. It is a spline function, made up of cubic polynomials,

$$\phi(r) = A_K(r-r_K)^3 + B_K(r-r_K)^2 + C_K(r-r_K) + D_K, \quad 2.35\text{Å} \leq r \leq 4.418\text{Å} \qquad (3)$$

where, over the range of interest, K runs from 1 through 8 and the r_k are the interatomic separations at which adjacent cubics are joined. The coefficients A_K, B_K, C_K, and D_K are shown in Table 1-A.

The Molière and Englert functions are spliced together with the function

$$\phi(r) = A(r-r_1)^5 = B(r-r_1)^4 + C(r-r_1)^3 + D(r-r_1)^2 + E(r-r_1) + F, \quad (4)$$
$$1.55\text{Å} \leq r \leq 2.35\text{Å}$$

where the coefficients are chosen so that the potential and its slope and curvature are continuous at r=1.55Å and 2.35Å. The coefficients A, B, C, D, E, and F are shown in Table 1-B.

As is typical in atomistic simulations, the crystal is treated in this study as consisting of two regions. There is an inner region of discrete atoms, each with a full complement of neighboring lattice sites within the range of the potential, and an outer region of infinite elastic continuum. Between the two, at the lattice-continuum interface, atoms lack a full complement of neighbors and, hence, require special (constant-pressure, Hookian and viscous) forces to augment the interatomic forces. For this study, the lattice is made up of 36 nearly octagonal (112) planes, with each plane containing 164 atoms. This approximately cylindrical lattice is about 55Å in diameter and 25Å thick. Atoms within a third neighbor distance of the edges of the lattice are designated as being at the lattice-continuum interface.

When analyzing a displacement cascade, it is very inefficient to integrate the equations of motion for all the atoms in the lattice each time step, since during most of the cascade evolution only a small fraction of the atoms move. To increase efficiency a subroutine was written and added to COMENT which enables the user to specify the

size and shape of a "mini-lattice" within the lattice. The mini-lattice may be either a spherical or cylindrical volume surrounding the evolving cascade. Like the lattice itself, the mini-lattice contains interior and (fixed) interface atoms. The equations of motion are solved only for the interior atoms of the mini-lattice. As the cascade develops the size of the mini-lattice is expanded as needed. The procedure employed is as follows:

1. The location of the PKA and its energy and direction are specified, and the center of the coordinate system is defined as the initial site of the PKA.

2. The shape, origin (a point or line which need not coincide with or pass through the center of the coordinate system), and radius of the mini-lattice are chosen to suit the anticipated cascade geometry.

3. Each time step, every atom which is more than r_{cm} (=.32Å) from its lattice site is checked to determine its position relative to the mini-lattice interface. If such a displaced atom is within r_{co} (=3.62Å) of the surface, the radius of the mini-lattice is increased (usually in steps of 1.5Å) and its center is relocated to a point midway between the origin and the position of the most energetic atom.

4. Once the mini-lattice is enlarged and relocated, the procedure outlined in (3.) is repeated until the energy of the most energetic atom falls below ESET ($\leq$8eV). At this point, the mini-lattice is enlarged for the last time, and, in addition, a layer of "damped" atoms 4.4Å thick is set between the interior and interface atoms of the mini-lattice to absorb energy flowing out from the cascade. In practice, the mini-lattice is so large near the end of the calculation that seldom more than several eV flows through this layer before phases one and two of the cascade are complete.

All cascades described in this report are in the process of being filmed. That is, for each cascade, the coordinates and energies of all moving atoms were recorded each time step and stored. A specially written computer code OSCAR is being used to organize this data and prepare it for plotting and filming with an FR80 Computer Output Microfilm Unit.

C. RESULTS

1. Frenkel Pair Stability

A number of static calculations have been carried out in order to determine, for the potential used in this study, the stability of isolated Frenkel pairs with different vacancy and interstitial orientations and separations. First the atomic configurations and configurational energy for an isolated vacancy and an isolated interstitial were calculated, then various Frenkel pairs were analyzed.

As expected, the vacancy formation energy was found to be 1.097 eV, in agreement with the value reported by Englert et al.[8] The formation energies for isolated interstitials in the crowdion and split configurations (these are "dumbbell" configurations centered on a lattice site and parallel to the <110> and <100>, respectively) were calculated to be 5.299 and 5.694 eV respectively. These formation energies are rather high compared with values obtained with other potentials.[4]

A table of Frenkel pair stability is, of course, a considerable aid in the evaluation and interpretation of computer simulated displacement cascades. Table 2 shows the stable and unstable configurations for all unique pairs with separations out through the ninth neighbor distance. It should be noted that at the completion of phases one and two of cascade evolution, interstitials tend to

be in the crowdion configuration and only rarely in the split configuration. Occasionally interstitials are found in the lowest energy configuration, the <111> split (E_I^F=5.106 eV), but never in the octahedral configuration (E_I^F=5.287 eV).

2. Cascade Evolution

A matrix of six PKA energies and twelve PKA directions was investigated and a total of approximately one hundred cascades were simulated. Of the twelve directions considered, six are low index directions (i.e., two near each of the principal axes) and six are high index directions (i.e., in the central region of the fundamental triangle shown in Figure 1). Table 3 summarizes the variations in the number of Frenkel pairs and the number of replacements with PKA direction and energy. Weighting the results in each direction equally, average numbers of Frenkel pairs and replacements per PKA were calculated for each PKA energy. The averages are included in Table 3. The following is a brief discussion of the results from the investigation of low and high index directions (see Figure 1).

Low index cascades are characterized by their tendency to produce long replacement sequences. At the lower energies ($\geq$75 eV) the <110> sequences are longest and focus most readily, while the <100> sequences tend to be shorter and more difficult to focus; no <111> sequences form. At higher energies (>75 eV) the <110> and <100> sequences rapidly defocus, and <111> sequences form. As is to be expected, the energy losses per collision increase rapidly in going from <110> to <100> to <111> replacement sequences.

One of the most interesting features of <110> cascades is that once a replacement sequence is initiated it tends to continue to propagate at low energies. For example, a 25 eV PKA in

the <110> direction produces a Frenkel pair with fourteen replacements; the last five replacements acquire kinetic energies of less than 5 eV. A filmed account of the event shows nicely how the combination of the momentum of the sequence and the squeezing down of window atoms behind displaced atoms tends to push the propagating sequence forward.

High index cascades are characterized by the tendency of the PKA to rapidly distribute its energy among several near neighbors. On the average, at lower energies ($\leq$75 eV) few Frenkel pairs or replacements form and the replacements are not in a focused sequence, while at higher energies (>75 eV) the number of Frenkel pairs and replacements increase and a few focused replacement sequences appear.

Perhaps the most noteworthy features of these cascades are (1) the number of Frenkel pairs tends not to be a monotonicly increasing function of PKA energy for a given direction, and (2) although the number of replacements increases rapidly with PKA energy, few occur in long sequences. These are believed to be related manybody effects which result from the tendency for energy deposited by high index PKAs to flow away from the region of deposition more slowly than energy deposited by low index PKAs. That is to say, thermal spikes form which may enhance annihilation at one PKA energy and clustering at another.

D. CONCLUSIONS

At most energies the number of Frenkel pairs per PKA is largest for PKAs with polar angles in the range 85 to 90°. Although the number of Frenkel pairs is not a monotonicly increasing function of PKA energy in all directions, the average number is monotonicly increasing. The variation in the average number of Frenkel pairs with PKA energy is not linear, however, which is not surprising considering the energy range investigated.

E. REFERENCES

1. D. G. Doran and J. O. Schiffgens, "Cascade Annealing - An Overview", HEDL-SA 874, April 1976 (to be published in the Proceedings of the Workshop on Correlation of Neutron and Charged Particle Damage, June 8-9, 1976 at Oak Ridge National Laboratory, Oak Ridge, Tenn.).

2. J. B. Gibson, A. N. Goland, M. Milgram, and G. H. Vineyard, Phys. Rev. 120, 1229 (1960).

3. J. O. Schiffgens and K. E. Garrison, J. Appl. Phys. 43, 3240 (1972).

4. J. O. Schiffgens and D. H. Ashton, J. Appl. Phys. 45, 1023 (1974).

5. I. M. Torrens and M. T. Robinson, in Interatomic Potentials and Simulation of Lattice Defects, P. C. Gehlen, J. R. Beeler, Jr., and R. I. Jaffee, eds., Plenum Press, NY 1972, p. 423.

6. M. T. Robinson and I. M. Torrens, Phys. Rev. 9, 5008 (1974).

7. P. Jung, R. L. Chaplin, H. J. Fenzl, K. Reichelt, and P. Wombacher, Phys. Rev. B 8, 553 (1973).

8. A. Englert, H. Tompa, and R. Bullough, in Fundamental Aspects of Dislocation Theory, J. A. Simmons, R. deWit and R. Bullough, eds., NBS Special Pub. 317, 1, (1970).

TABLE 1-A

POTENTIAL PARAMETERS

The Coefficients for the Long Range Part of the Pair Potential for Copper
(See Equation 3)

K	$r_K(\mathring{A})$	$A_K(\frac{eV}{A^3})$	$B_K(\frac{eV}{A^2})$	$C_K(\frac{eV}{A})$	$D_K(eV)$
1	2.0	-3.2382	6.3981	-4.4591	0.8453
2	2.551	-0.258148	1.045285	-0.357854	-0.210930
3	3.061199	-2.221407	0.650164	0.507164	-0.155699
4	3.341810	1.507669	-1.219882	0.347295	-0.011272
5	3.607658	-0.080144	-0.017445	0.018353	0.023168
6	4.209149	2.186182	-0.162063	-0.089620	0.010455
7	4.311190	-1.575972	0.507171	-0.054405	0.001945
8	4.418461	0.0	0.0	0.0	0.0

TABLE 1-B

POTENTIAL PARAMETERS

The Coefficients for the Intermediate Part of the Pair Potential for Copper
(See Equation 4)

$r(\mathring{A})$	$A(\frac{eV}{A^5})$	$B(\frac{eV}{A^4})$	$C(\frac{eV}{A^3})$	$D(\frac{eV}{A^2})$	$E\frac{eV}{A})$	F(eV)
1.55 to 2.35	-16.386201	20.607837	-9.105818	4.437922	-3.235393	0.685515

TABLE 2

FRENKEL PAIR STABILITY

Nearest Neighbor	Crowdion Interstitial* Vacancy Coordinates			Pair Condition	Split Interstitial** Vacancy Coordinates			Pair Condition
1st	0	1/2	1/2	Unstable	1/2	0	1/2	Unstable
	1/2	0	1/2	Unstable	1/2	1/2	0	Unstable
	0	-1/2	1/2	Stable				
2nd	0	0	1	Stable	0	0	1	Unstable
	1	0	0	Stable	1	0	0	Stable
3rd	1/2	1/2	1	Unstable	1/2	1	1/2	Unstable
	1	1/2	1/2	Stable	1/2	1/2	1	Stable
	1/2	-1/2	1	Stable				
	1	-1/2	1/2	Stable				
4th	0	1	1	Unstable	1	0	1	Unstable
	1	0	1	Unstable	1	1	0	Stable
	0	-1	1	Stable				
5th	0	1/2	3/2	Stable	0	1/2	3/2	Stable
	1/2	0	3/2	Stable	0	3/2	1/2	Stable
	0	-1/2	3/2	Stable	3/2	1/2	0	Stable
	3/2	0	1/2	Stable				
6th	1	1	1	Stable	1	1	1	Stable
	1	-1	1	Stable				
7th	1/2	1	3/2	Stable	3/2	1/2	1	Stable
	1	1/2	3/2	Stable	1/2	1	3/2	Stable
	3/2	1/2	1	Stable	3/2	1	1/2	Stable
	3/2	-1/2	1	Stable				
	1	-1/2	3/2	Stable				
	1/2	-1	3/2					
8th	2	0	0	Stable	2	0	0	Stable
	0	0	2	Stable	0	0	2	Stable
9th	1/2	1/2	2	Stable	1/2	1/2	2	Stable
	0	3/2	3/2	Unstable	1/2	2	1/2	Stable
	3/2	0	3/2	Stable	3/2	0	3/2	Unstable
	1/2	-1/2	2	Stable	3/2	3/2	0	Stable
	2	1/2	1/2	Stable				
	2	-1/2	1/2	Stable				
	0	-3/2	3/2	Stable				

*The interstitial straddles the center of the coordinate system with a crowdion <011> configuration.

**The interstitial straddles the center of the coordinate system with a split <001> configuration.

TABLE 3-A

SUMMARY OF LOW ENERGY CASCADES

NUMBER OF FRENKEL PAIRS[†]

PKA Energy (eV)		25	50	75	100	150	200
PKA Direction							
Polar	Azimuthal						
(degrees)							
123.5 (56.5)	44.0	0	1	1	1	1	1
62.5 (117.5)	40.0	0	0	1	1	1	1
67.5	40.0	0	0	1	1	2	1
85.0	320.0 (40.0)	1	1	1	1	1	2
89.0	316.0 (44.0)	1	1	1	2	2	3
85.0	17.5	1	0	1	2	1	4
85.0	10.0	1	1	1	2	1	3
89.0	1.0	1	1	1	1	1	3
75.0	20.0	0	1	1	1	2	3
70.0	27.5	0	0	1	1	2	2
80.0	30.0	0	1	1	0	1	2
75.0	35.0	0	0	1	1	2	1
Average		0.4	0.6	1.0	1.2	1.4	2.2

[†]The total number of vacancy-interstitial pairs are listed here, regardless of whether the vacancies or interstitials are clustered at the termination of the calculation. When there is no atom within 1.5 Å of a lattice site, COMENT identifies the site as a vacancy. Correspondingly, when any two atoms are within 1.3 Å of a given lattice site, and only this site, the atoms are identified as an interstitial and the site as an interstitial site.

TABLE 3-B

SUMMARY OF LOW ENERGY CASCADES

NUMBER OF REPLACEMENTS

PKA Energy (eV)		25	50	75	100	150	200
PKA Direction							
Polar	Azimuthal						
(degrees)							
123.5 (56.5)	44.0	0	1	1	2	4	∿9
117.5 (62.5)	40.0	0	2	4	1	3	6
67.5	40.0	0	2	2	2	5	9
85.0	320.0 (40.0)	8	7	4	7	10	17
89.0	316.0 (44.0)	13	∿21	10	8	7	18
85.0	17.5	1	4	5	6	∿15	22
85.0	10.0	2	2	1	10	7	∿25
89.0	1.0	3	6	3	3	∿20	∿20
75.0	20.0	2	2	2	7	8	∿21
70.0	27.5	0	0	0	2	7	∿8
80.0	30.0	0	1	3	4	15	13
75.0	35.0	0	0	5	7	11	21
Average		2.4	4.0	3.3	4.9	9.3	15.8

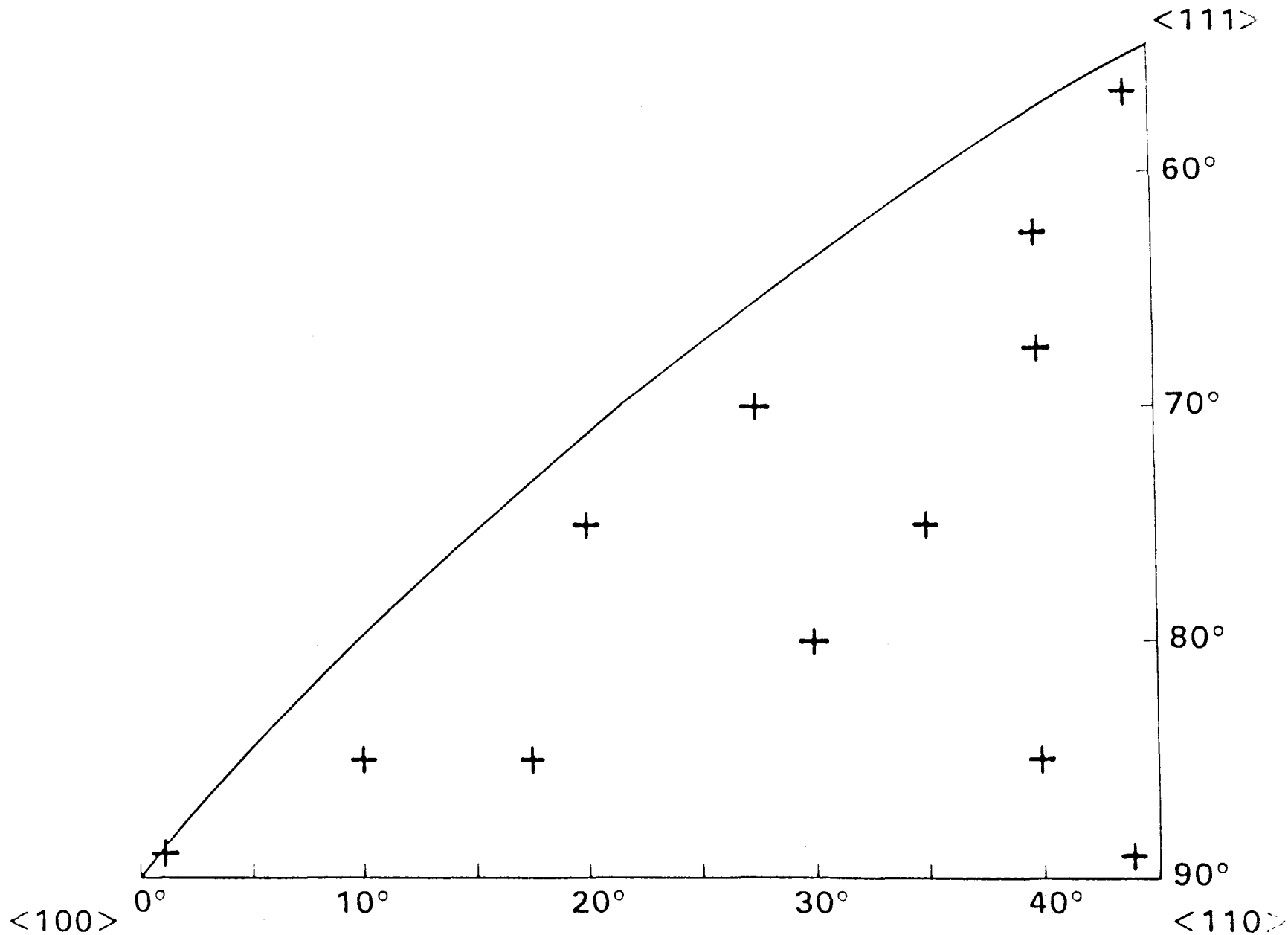

FIGURE 1. The Fundamental Triangle, Where the Crosses (+) Show the PKA Directions Investigated in This Study.

COMPUTER SIMULATION OF SHORT-TERM DEFECT ANNEALING

D. M. Schwartz (California State University, Northridge), P. Goldstein (BCS-Richland), and D. G. Doran/W. M. McElroy (HEDL)

The computer simulation of displacement cascades of energy greater than several keV is currently carried out in two steps corresponding to different time frames. The first step is the formation of a high local concentration of defects in a configuration that is stable over a time interval ($\sim 10^{-11}$ sec) that is too short to permit thermal migration of the defects. The second step, usually called "short-term annealing", simulates the thermal migration of the defects. Their interactions result in the annihilation of unlike defects, clustering of like defects, and the escape of some mobile defects from the vicinity of the cascades.

The short-term annealing simulation code (HAPFCC) used in previous work at HEDL utilized a rather detailed description of the migration of small defect clusters, resulting in a slow computational speed. Two major changes have been made to develop a faster code. One was to simplify the descriptions of the defects, their motion, and their interactions. The other was to change the manner in which the program progresses; in particular, the use of time steps as in HAPFCC was abandoned.

The SCAS Code uses three random numbers, two to select the mobile defect and one to select the jump vector. To aid the search for defects with which the jumping defect might interact, the crystal is subdivided into slabs. The code was designed to optimize run time and storage and contains several unique features which make this possible:

1. String structures are used to link defects of the same type and size or defects belonging to the same crystal slab. This speeds up the mobile defect selection process and the search for neighboring defects without a great cost in additional storage.

2. An array is used from which the type of defect to make the next jump is selected; its mode of construction ensures that a jump can occur every time. The program run time is thus made independent of the actual elapsed time between jumps and the simulation procedure can, in principle, be carried to completion in a single run for all types of mobile defects. A calculated total elapsed real time is continually updated.

3. Locations vacated by an annihilated defect are linked to a free storage pool which operates as an internally linked first-in-first-out stack. The result is an efficient mode of dynamic storage.

The present version of the program permits the use of 1000 defects of two different types (vacancy or interstitial) and any cluster size from 1 to 100. Of these types and sizes, up to 20 different small clusters can be mobile.

The SCAS code has been debugged and documented in draft form.

RADIATION DAMAGE ANALYSIS AS APPLIED TO FUSION REACTOR FIRST WALLS

G. R. Odette (UCSB) and D. G. Doran/W. N. McElroy (HEDL)

A. INTRODUCTION

Clearly, it will be some time before an irradiation facility will be available which closely approximates fusion first wall (FFW) conditions and is able to provide an adequate base of engineering irradiation effects data. Hence, interim estimates of FFW behavior will be based on extensive fission reactor and charged particle simulation data along with a limited amount of data from present and proposed high energy accelerator based environments (ABE). Optimal use of this set of less than ideal environments requires development and application of damage analysis tools. This report will briefly discuss damage analysis as applied to FFW damage assessment and indicate some directions of needed development. It is hoped this will stimulate further discussion on this important topic.

Three primary objectives of damage analysis are: (1) definition and quantification of significant damage variables; (2) correlation and interpretation of data taken in available environments; and (3) projection of damage response to new environments. In practice attempts at correlations and projections are usually made for a given set of material variables (i.e., type, composition, microstructure) and test conditions (i.e., property, test type, and temperature). Hence, the focus of damage analysis is on the effect of irradiation environment variables such as neutron flux-fluence-spectra, irradiation temperature, stress, and the chemical surroundings.

To accomplish the objectives of damage analysis involves three related tasks: (1) environmental monitoring (flux, fluence, and temperature measurement); (2) development of models and interpretation of experimental data to understand the underlying mechanisms of radiation

damage, hence their dependence on irradiation environment; and (3) systematic data correlation and projection to design (e.g., FFW) environments including estimates of projection uncertainties.

Critical differences between FFW conditions and available irradiation environments include: (1) transmutation generation rates, particularly helium and hydrogen; (2) periodic variations (pulsing) of neutron fluxes, temperatures and stresses; (3) primary knock-on atom (PKA) recoil spectra; (4) displacement damage rates; and (5) total (nominal) lifetime exposures. Although not always stated explicitly, the conceptual framework for the discussions in this report is a stainless steel FFW with a nominal loading of 1 MW/m^2.

Careful review of these factors makes it clear that it will not be possible to duplicate FFW conditions over a significant irradiation volume in any available or proposed test environment (short of an actual fusion reactor with appropriate wall loading and burn cycle).[1] This assessment can be made without even considering factors such as potential interactions between surface damage and bulk effects, and the existing ambiguities in design dependent FFW conditions.

This introduction closes with a few comments regarding the suitability of a distributed energy (d,n) neutron source vis-a-vis a 14 MeV monoenergetic source for FFW damage studies. Two questions have been raised. The first is whether a "pure" 14 MeV source is a necessity. The authors think not, for the following reasons. (1) Conceptual FFW spectra are distributed in energy with only $\sim$20% of the neutrons at 14 MeV. (2) The recoil atoms characteristic of displacement damage are distributed in energy even for monoenergetic neutrons. It is the recoil atom energy spectrum that is significant, not the neutron spectrum per se. In this regard, a 14 MeV source has no greater similarity to a FFW than does a properly selected (d,n) source. (3) The transmutation rate relative to the displacement damage rate in a FFW

can be more closely matched with a (d,n) source than with a 14 Mev source.

The second question concerns the uncertainties introduced by the presence in (d,n) sources of neutrons of energy >14 MeV. While the contributions of these neutrons to presently used spectral dependent damage parameters are indeed uncertain, they are small and do not preclude sufficiently accurate assessment of the utility of such sources.

In summary, comparisons of FFW environments with neutron irradiation environments must be based largely on parameters most directly related to damage production and not simply on considerations of neutron spectra.

B. ENVIRONMENTAL DEFINITION

There has been substantial progress in the last decade in characterizing neutron irradiation environments in fission reactors. Quoted relative integral flux spectral errors have been reduced from $\sim\pm 50\%$ to $\sim\pm 15\%$.[2] Accurate flux-spectral characterization is based on a marriage of sophisticated reactor physics calculations and multiple reaction rate spectrometry. Reaction rate, reaction cross section, and reactor physics information are combined in a spectrum unfolding analysis which can provide not only nominal flux- (or fluence-) spectra $\phi(E)$ but also estimates of associated errors $\delta\phi(E)$ due to data, measurement, and analytical uncertainties.

The flux-spectral errors can be used along with nominal defect cross sections (see Section C.1 on Production of Displacement Defects and Transmutants) to estimate dosimetry contributions to defect production rate uncertainties. A detailed study of this sort for a FFW spectrum showed relatively small errors of 10-15%.[3] Similar values are likely to be appropriate for displacement rates in fission reactors,

although helium and hydrogen production rate uncertainties are believed to be somewhat larger. Normal dosimetry errors for 14 MeV ABEs should contribute less than 10% uncertainty to nominal damage reaction rates. However, because of the large flux gradients, uncertainties due to positional variations may be larger.

Although positional dosimetry is absolutely necessary for (d,n) ABEs, there is currently a definite lack of reaction cross section and neutronic data of sufficient accuracy above $\sim$15 MeV. The impact of these inadequacies on defining defect production rates in such facilities should be determined from sensitivity studies. Fortunately, this problem can be resolved to a large degree by using integral reaction rate measurements in existing low intensity (d,n) sources whose flux-spectra have been accurately measured using time-of-flight techniques. That is, multiple reaction rate and calculational methods can be verified and calibrated in such available facilities.

C. DAMAGE MECHANISMS, MODELS, AND MODEL TESTING EXPERIMENTS

An important goal of radiation damage research is development of a comprehensive damage model which is quantitatively predictive of a broad range of experimental observations utilizing only a few adjustable parameters. However, current models do not include all relevant mechanisms and interactions between mechanisms nor are they quantitatively predictive. Presently lacking is a theoretical model sufficiently comprehensive that it provides a framework for testing and applying results obtained from narrower studies of specific phenomena.

The following discussion is not intended to review the current status of our theoretical understanding of radiation damage, other than to note that it is inadequate even for charged particle and fission reactor applications.[4] Rather, some of the critical differences between available and FFW environments will be discussed from a perspective of the current mechanistic understanding derived from damage

models (primarily based on rate theory) and an interpretation of an extremely limited amount of experimental data.

The discussion will be based on a phenomenological framework for a comprehensive damage model which would include stages of defect production, microstructural evolution, and microstructurally induced property changes.

1. Production of Displacement Defects and Transmutants

Primary defect production is probably most dependent on the flux-spectral variable. It is convenient to express the spectral dependence in terms of a defect production cross section $\sigma_j(E)$, where j is the defect type. These cross sections can be used along with flux-fluence-spectra to define physically based exposure parameters, such as displacements-per-atom (dpa), or defect production rates, such as free defects, to be used as damage parameters in more comprehensive damage models.

a. Displacement Defects - Displacement defect production cross section calculations are composed of two parts. First, the differential PKA production cross section, $\chi^t(E,T)$, is determined as a function of neutron energy E and PKA energy T using nuclear data and kinematics models. A secondary defect production function, $\nu_j(T)$, is then used with $\chi^t(E,T)$ to define

$$\sigma_j(E) = \int_0^{T^{mx}} \chi^t(E,T)\nu_j(T)dT. \qquad (1)$$

Computer simulation experiments have been used to derive $\nu_j(T)$ expressions for both total displaced atoms and for residual clustered and unclustered defects remaining after short-term intracascade annealing. Experimental and theoretical evidence suggests that the local structure of

defects following short-term annealing, as well as their numbers, is an important factor in determining the nature of radiation damage.

However, significant uncertainties remain in determining both $\chi^t(E,T)$ and $\nu_j(T)$ (especially the latter) due to data, parameter, and model uncertainties. This is indicated by substantial differences in the results of different investigators and, in some cases, apparent discrepancies between experiment and theory.

A review of displacement defect production cross sections for neutrons was recently completed[5] and the following conclusions were reached:

(1) Below neutron energies of about 14 MeV, nuclear data and nuclear kinematics models contribute a relatively small uncertainty, but above this energy nuclear data and kinematics become increasingly ill-defined. Charged-particle-out and multiple particle emission reactions increase in importance at higher energies and should be treated with the reasonably rigorous kinematic models which have been developed. Further, the compound nucleus treatment now utilized for inelastic and nonelastic events may not be fully appropriate at high neutron energies in some cases where direct or pre-equilibrium reactions are known to be important.

(2) The secondary defect production functions are model sensitive. Major sources of uncertainty are energy partition between atomic motion and electronic losses, the nature of the displacement and cascade formation process at low energies including the length of replacement sequences, gross cascade structure at high recoil

energies, and defect recombination and clustering criteria. Further, most available functions have been derived for PKA energies of 100 keV or less. These functions must be extrapolated to the several hundred keV recoil energy range characteristic of high energy inelastic reactions if calculations are to be extended up to and beyond 14 MeV neutron energies.

Current models are inadequate to predict the athermal formation of large vacancy loops in cascades as observed under some conditions. Nor are the very long replacement sequences deduced in some experimental studies obtained with current computer models -- whether this is a failure of the models remains to be seen.

(3) Ratios of spectral-averaged defect production cross sections are convenient measures of the relative efficiency of various environments for producing displacement defects. Comparing pure 14 MeV to pure fission spectrum neutrons, this ratio ranges from $\sim$1.5 to 3 depending on the material, defect type, and secondary defect production model. Comparing FFW and fission spectra the ratio is $\sim$1.3 to 2.2.

(4) There have been a number of experiments, monitoring changes in different properties, aimed at deducing a ratio of 14 MeV to fission spectrum damage.[6] The results range from 3 to 20, hence are consistent only in some cases with the simple assumption that property changes are proportional to the number of defects. In interpreting such data it is critical that the experimental conditions, especially temperature, and the effect of specific defects on the particular property being monitored be explicitly considered in the analysis.

Further, very precise dosimetry is necessary if quantitative conclusions are to be drawn. It is questionable whether definitive conclusions can be made as yet from these results regarding the adequacy of damage models.

(5) A major difference between fusion and fission environments is a much larger cross section in the former for the production of very high energy recoils (e.g., >1 MeV in ^{93}Nb) due to heavy charged-particle-out reactions such as (n,α). However, except for special cases (e.g., Ni) the contribution of high energy events to total displacements is small.

Additional computer simulation of displacement cascades and cascade annealing and fundamental experiments are clearly called for. Current programs are aimed at achieving a better understanding of the low energy regime in which many-body interactions must be treated, and of the high energy regime describable as a series of binary collisions, and how they merge. To encompass the fusion reactor regime such calculations must be extended to recoil energies of several hundred keV. In addition, such simulations will generally require inclusion of additional physics before direct ties can be made with experiment.

Finally, extension of defect production cross section calculations to very high neutron energies (>15-20 MeV) for damage analysis of (d,n) ABEs will require development of more accurate nuclear data and models.

b. Transmutation Production - Production rates of gaseous helium and hydrogen and chemical transmutants from alloy constituents and impurities can be directly calculated from

reaction cross sections and ancillary nuclear data. The current data base is certainly not complete or highly accurate but is probably sufficient for FFW, 14 MeV ABE and fast reactor applications. Thermal reactor irradiations of nickel-bearing alloys produce copious amounts of helium via the two-stage $^{58}Ni(n,\gamma)^{59}Ni(n,\alpha)^{56}Fe$ reaction. Calculations of thermal reactor helium production agree with empirical correlations to within about a factor of 2.

For the (d,n) ABEs the data base is entirely inadequate. Fortunately this should not be a problem in the case of helium, since available low intensity (d,n) sources can be used to study integral helium generation rates using the isotope dilution mass spectrometry method.[7] Proton recoil and radiochemical methods might also be used in these environments to study hydrogen production rates. Chemical transmutant production will probably remain uncertain until high exposure chemical and mass spectrometric experiments are carried out in all relevant environments.

c. Total Defect Production Rate Uncertainties - Uncertainties in defect production stem from both flux-spectral errors $\delta\phi(E)$ and uncertainties in defect production cross sections, $\delta\sigma_j(E)$. Sensitivity studies to assess the magnitude of sources of error due to both these contributions should be made, particularly for the (d,n) ABE. Such studies are underway but no results are currently available.

It is important to maintain a perspective on defect production uncertainties. If these parameters are intended to provide exposure units for data correlation, relative rather than absolute values are of primary interest. However, if the parameters are for input to comprehensive damage models or analysis of particular experiments, absolute

defect production values are of interest; in this case secondary defect production models are likely to be the major source of uncertainty.

2. Microstructural Evolution

At elevated temperatures characteristic of reactor irradiations, defect production is only the first step in the formation of extended irradiation defect microstructures consisting of bubbles, voids, dislocations (both loops and network), precipitates and regions of alloy constituent or impurity segregation. The microstructural evolution stage comprises three phenomena: diffusion of mobile defects to sinks, nucleation of extended defects, and growth of extended defects.

Current models of microstructural evolution, largely based on rate theory,[8] suffer three principal deficiencies: (1) they do not include all relevant damage mechanisms and interactions between mechanisms, that is, the models are not sufficiently comprehensive; (2) modeling of individual mechanisms is often based on sets of simplifying assumptions which may not be valid; and (3) results are sensitive to material and defect parameters which are often not precisely known. Hence, it is not surprising that model based calculations are only qualitatively predictive of experimental observations.

Intensive study is being given to some aspects of microstructural evolution modeling including: (1) identification of critical rate controlling steps; (2) determination of sink strengths and bias factors as influenced by local structure and composition; (3) kinetics of correlated, defect-solute atom diffusion and solute segregation; (4) the thermodynamics and kinetics of steady state, homogeneous nucleation; and (5) refinements of rate theory to account parametrically for stress, trapping effects, vacancy loops from cascade collapse, and temperature cycles.

The authors believe that too little attention is being paid to the following items: (1) assessment of the basic validity of rate theory; (2) development of comprehensive microstructural evolution models including diffusional, nucleation, and growth stages; (3) heterogeneous nucleation; (4) details of defect-defect and defect-solute atom interactions (such as trapping, correlated diffusion, vacancy-interstitial annihilation and interstitial pop-out of substitutuional helium atoms) and defect properties (such as small cluster thermodynamics and defect diffusivities); (5) detailed treatment of dislocation structure evolution; and (6) derivation of model parameter groups which can be unambiguously defined in carefully controlled experiments.

With this as prologue, the problem of going from available test environments to FFW environments will be discussed in terms of the differences mentioned previously.

a. Displacement Damage Rate Effects - Agreement between rate theory descriptions of damage rate effects and experiment has not always been good.[9] First order effects of damage rate are the result of defect-defect interactions (e.g., vacancy-interstitial recombinations) and thermal emission of defects (e.g., vacancy emission from voids). Correlated diffusional interactions of self interstitials and vacancies with solute atoms or transmutant gases are also rate sensitive as is the influence of intra-cascade vacancy loop formation. Thermal emission effects are most critical for small clusters, hence for the nucleation stage of microstructural evolution. The growth stage is also rate sensitive due to emission at higher temperatures. Again standard nucleation and growth theories account, in principle, for rate effects. However, quantitative predictions will require detailed knowledge of defect-interaction and material parameters and the inclusion of all relevant mechanisms in more comprehensive damage models.

Displacement rate effects are clearly dependent on irradiation temperature. It is important to realize that different phenomena (e.g., nucleation or growth) will generally respond differently to damage rate changes. Hence unique temperature corrections are not likely to be successful.

b. Pulsing Effects - First order effects of irradiation pulsing in FFWs include enhanced vacancy-interstitial recombination relative to steady state irradiations at the same net damage rate, and thermal annealing of defects between pulses. These factors could reduce void growth and might significantly reduce void nucleation under some circumstances. However, substantial drops in temperature and increases in stress levels between fusion burns might, in contrast, increase void nucleation rates. Second order effects such as cascade (or vacancy loop) overlap and dislocation restructuring during stress pulses might also be significant.

Preliminary efforts to study some of these effects have revealed that rate theory modeling of pulsing phenomena is possible but involves complex mathematics.[10,11] The authors believe models can be developed, in conjunction with pulsing experiments, which will allow for reasonable correlation of pulsed and steady state data.

c. PKA Cascade Effects - The bulk of the evidence suggests that no particular surprises are likely in going from fission reactor to FFW PKA spectra. The currently most interesting question involves the spectrum and temperature dependence of the formation of transient vacancy loops in cascades. At lower temperatures these loops would be long-lived so would serve as point defect sinks, hence lowering

nucleation and growth rates of extended defects such as voids.[12] Proper accounting of this influence is necessary for correlating both neutron-neutron and neutron-charged particle data. Some transient cascade clusters presumably maintain a three dimensional morphology; these can enhance void nucleation under some conditions.[13]

Cascade loop formation may be more probable at the high PKA energies found in FFW environments. It is important, therefore, that the efficiency and characteristics of loop formation as a function of PKA energy be understood. An optimal approach to such understanding might be found in a marriage of computer simulation studies and semi-empirical damage function analysis of experimental data (see Section D on Semi-Empirical Data Correlation Methods), as is presently being carried out in the breeder reactor program.

d. Total Damage Exposures - There are at least four broad exposure regimes of interest: (1) low exposures (typically $<<$ 1 dpa) for study of primary defect production; (2) nucleation exposures (typically $<$ 10 dpa) where a stable extended defect microstructure is formed; (3) a quasi-steady state exposure regime ($<$ 50-100 dpa) where growth can usually be described by a power law type behavior; and (4) a growth saturation regime ($\gtrsim$ 100 dpa) which is theoretically predicted but has not generally been observed. If microstructural changes saturate only beyond an unacceptably high level, as current data suggests for some materials (e.g., stainless steel), the fourth regime is of only academic interest to engineering design. Although some data extending to FFW lifetime design exposures is essential, much can be learned about the underlying damage mechanisms by studying nucleation microstructures at moderate exposures ($<$ 20 dpa) and the influence of such microstructures on

subsequent growth behavior. The incorporation of this information into advanced damage analysis models should permit the projection of damage response from test to FFW environments.

e. Transmutants Other Than Helium - Two significant classes of transmutants (other than helium) are gases with a relatively high solubility and mobility, such as the isotopes of hydrogen, and solid chemical transmutants. Hydrogen could influence the microstructural evolution by altering surface energies (stacking faults or void surfaces) and by forming relatively insoluble molecules such as CH_4 which sould stabilize small vacancy clusters (see discussion of Helium Effects). Chemical transmutants may also be significant, particularly if solid solution products believed to reduce swelling are produced.

f. Helium Effects - Several extensive discussions of the influence of helium on microstructural evolution have been reported, although both reliable modeling and experimental information are very scarce.[15-18] Following is a summary of some tentative hypotheses.

(1) Interactions between displacement defects and helium will influence the mobility of both species. Trapping by helium atoms may reduce the mobilities of vacancies and interstitials, while competing reactions involving pop-out of trapped helium via vacancy-interstitial recombination may increase helium diffusivity. The effective diffusivities of all mobile species, including small bubbles, significantly influence stages of nucleation and growth.

(2) The effect of helium on void nucleation is dependent on the temperature, damage rate, microstructure and material parameters. At intermediate temperatures ($\sim$ 500-600°C) voids nucleate on a distribution of bubbles which have previously nucleated and grown to a sufficient size to promote void nucleation. (Bubbles are clusters of helium and vacancies which have radii such that they grow only with the addition of helium atoms at prevailing conditions, while voids are gas-vacancy clusters which have radii such that they have a continuous positive growth rate. The term cavity is used for either a void or a bubble.) Steady state models involving constant fluxes of both helium and displacement defects corresponding to the total helium concentration are not appropriate for neutron irradiation conditions.[19]

Microstructures at the end of the nucleation stage may consist of primarily bubbles, primarily voids, or mixtures of voids and bubbles. Important microstructural parameters are the total cavity density and the ratio of voids to bubbles. If a high density of small bubbles forms initially, void nucleation may be suppressed since the bubbles may be too small to promote nucleation but may act as neutral sinks to decrease net vacancy fluxes. Hence, although increasing helium generation rates increases the cavity density it may increase or decrease the void density.

The nucleation and growth of bubbles may be influenced by the presence of both irradiation induced extended defects, such as dislocation loops, and by point defects. Decreased bubble density would result from increased helium diffusivity under irradiation, resolutioning of small bubbles by displacement cascades or

interstitial impingement, and diffusional bubble coalescence driven in part by irradiation induced defects.

Part of the incubation dose (exposure before the onset of measurable swelling) is probably due to the time it takes to grow nucleation sites. Higher helium generation rates would tend to reduce incubation times if conditions were amenable to void nucleation and growth.

The evolution of the dislocation microstructure may also be influenced by helium. Some evidence indicates that helium promotes the nucleation of dislocation loops. This would have a significant influence on the evolution of void microstructures. No quantitative studies of this effect have been made to date.

It is noted that controlling nucleation is probably the most effective means of influencing damage microstructures.

(3) The cavity growth regime is influenced by helium both directly and through the nucleation microstructure discussed previously. The basic features of diffusion limited void swelling behavior can be illustrated in the simple equation for the swelling rate $\dot{s}$

$$\dot{s} \simeq \frac{G_d M \varepsilon f}{(1+M+Q)^2} - E_v^v \qquad (2)$$

where G_d is the displacement rate; ε is the dislocation bias; M is the ratio of the dislocation sink strength ($\simeq$ dislocation density, ρ_d) to the void sink strength

K_v^v ($\simeq 4\pi r_v N_v$ where r_v is the void radius and N_v is the void density); Q is the ratio of bubble to void sink strength; f is the fraction of vacancies reaching sinks (i.e., not recombining); and E_v^v is the void vacancy emission rate ($\simeq K_v^v D_v \overline{C_v}$ where D_v is the vacancy diffusivity and $\overline{C_v}$ the equilibrium vacancy concentration at a void surface). The first term in Equation 2 represents partitioning of vacancies to voids and the second represents vacancy emission from voids. A preliminary set of growth calculations has indicated the following effects of helium generation rate on void swelling. At lower temperatures the swelling rate can be increased by increasing the void densities resulting from high helium generation rates, since this increases f and decreases M towards an optimal swelling value of 1. At intermediate to higher temperatures increasing the void density can decrease swelling, due to enhanced vacancy emission by smaller voids (i.e., because of their higher densities and smaller size, E_v^v is increased), and due to bubbles remaining stable and acting as point defect sinks, thus increasing Q (i.e., vacancies which would otherwise go to voids are lost at bubbles). Other helium related factors would appear to reduce swelling under some circumstances. Of course the preceding results are sensitive to model assumptions and choice of parameters.

Potential mechanisms for increased void swelling due to high levels of helium production include (1) promotion of nucleation of voids under conditions in which nucleation would not otherwise occur, and (2) decreased vacancy emission due to a lower $\overline{C_v}$; that is, small voids which would otherwise anneal can be partly stabilized by internal gas pressure.

Another component of incubation time, the delay associated with very small voids growing to observable sizes, might be increased or decreased by helium according to the mechanisms discussed.

Hence, the net effect of increased helium generation rates on cavity growth at intermediate temperatures depends on particular conditions, including the intrinsic (intrinsic refers here to fast reactor conditions) swelling characteristics of the material (e.g., in low swelling materials added helium would increase swelling, while in materials with larger swelling rates helium might decrease swelling).

At high temperatures cavities have a predominately bubble character. At high helium concentrations bubble swelling can be significant, particularly at low bubble densities. The general characteristics of bubble swelling can be simply described by

$$s \simeq C_1 \, G_{He}^{1.25} \, D_{He}^{.25} \, T^{3/2} \, t^{3/2} \qquad (3)$$

where C_1 is a constant of proportionality, G_{He} the helium generation rate, D_{He} the helium diffusivity, T the temperature and t the irradiation time.[20] These model predictions are based on the following simplifying assumptions: two-atom clusters of helium are taken as stable bubble nuclei, the bubbles are taken to be immobile (collisional coalescence is not considered), and bubbles are taken to be in continuous thermal equilibrium. The role of irradiation induced displacement damage in influencing bubble swelling, e.g., through resolutioning, is not treated.

Finally, it is noted that, at high temperatures, helium will act in combination with an external stress exceeding a critical magnitude to promote swelling by unstable cavity growth.[21]

(4) Much of the uncertainty discussed previously could be eliminated if an adequate set of data were available. The very limited data which does exist falls into three general classes. (1) Ion, electron and neutron irradiations of materials preinjected with helium or other noble gasses have been conducted. Most of these experiments indicate an increased cavity density and unchanged or diminshed net swelling with increasing gas concentration. In some cases essentially no void swelling was observed if small helium bubbles were initially present.[22] A series of preinjection experiments by Mazey and Nelson demonstrated the importance of the distribution of helium.[23] For cases of ambient temperature injection and formation of only small bubbles, subsequent ion bombardment produces swelling that is relatively insensitive to the helium level. However, if the helium is preinjected in samples at high temperatures, producing a lower density of larger bubbles, swelling is increased at large helium levels in subsequent ion bombardments. (2) Simultaneous ion bombardment and helium injection has been carried out in a few experiments. Experiments conducted at relatively high displacement rates showed little effect of helium on net swelling.[24] Irradiations at lower dose rates showed substantial enhancement of early, homogeneously distributed, void nucleation with increasing helium injection rates (under circumstances in which nucleation either did not take place or occurred heterogeneously late in the irradiation in

the absence of helium injection).[25] However, the net swelling did not change significantly (actually decreasing slightly at the highest injection rate) in the case where voids nucleated with or without helium. (3) Thermal reactor irradiations of aluminum doped with lithium, in which copious amounts of helium are produced, have indicated that at very high helium concentrations (2000 appm) the net swelling is not significantly altered relative to undoped aluminum at equivalent dpa values.[26] In the lithium doped specimens the swelling is predominately due to helium bubbles. Again the total cavity density increased with increasing helium concentration.

Thermal reactor (HFIR) irradiations of a low swelling heat of stainless steel have been performed in which large concentrations of helium (∿3500 appm) and displacements (∿50 dpa) were produced.[27] The results indicate a substantially enhanced total swelling in the HFIR compared with fast reactor irradiation (∿15 ppm He and ∿35 dpa) for both cold worked and solution-annealed specimens irradiated above 500°C. The total cavity density was increased about an order of magnitude in the HFIR case and a somewhat different morphology of other defect microstructures (precipitates and dislocations) developed. The swelling was insensitive to temperature below 550°C but increased substantially with temperatures above 550°C; it appears to be predominately due to bubbles.

All the data outlined above are qualitatively consistent with the general picture given here of the influence of helium on void swelling. However, it should

be clear that none of the results from the three classes of experiments are directly applicable to FFW damage assessment because of the large variations in irradiation variables from conceptual design values. Matching FFW helium-to-dpa ratios and levels in accelerated ion bombardment studies to various neutron environments does not guarantee a similar damage response. The helium-to-dpa ratio is time dependent in thermal reactor irradiations of stainless steel (impurities such as boron may alter the time dependence and distribution) and this may also influence nucleation phenomena, precluding direct simulation of fusion first wall conditions. However, FFW conditions can be approximated by employing a sequence of spectral tailorings.

(5) The preceeding review indicates the complexity and uncertainty associated with the effects of simultaneous generation of displacement defects and helium on the damage microstructure. Clearly, damage response is sensitive to a number of variables and there are indications that increasing levels of helium can either increase or decrease net swelling depending on the specific conditions.

The authors are developing a comprehensive model of helium effects on microstructural evolution which should, along with additional experimental data, clarify the situation considerably. However, particular pieces of the model such as migration of helium during irradiations, bubble nucleation, the influence of helium on the dislocation structure and a number of others must be more fully understood before quantitative predictions are possible. An important role of a

comprehensive model is, indeed, to provide a framework for assessing the significance of proposed damage mechanisms.

(6) In spite of the clear inability to make reliable quantitative predictions, the authors would like to speculate a bit more on swelling in FFWs relative to HFIR and EBR-II data. The admittedly incomplete list of effects discussed in this paper suggest that, above 500-550°C for stainless steel, FFW cavities will be predominantly bubbles rather than voids. If one assumes that only bubble swelling will occur in a FFW, the net swelling would be only about 10% of that in HFIR at equivalent dpa levels (50 dpa) for the same bubble density. Using this scaling, first wall swelling of <2% would be predicted from HFIR data, a magnitude roughly consistent with that found for void swelling of stainless steel in fast reactors. This suggests that HFIR data is likely to provide a conservative basis for predicting swelling under FFW conditions.

3. Influence of Damage Microstructure on Mechanical Properties

Surprisingly little work has been done on modeling or deriving empirical correlations between damage microstructures and mechanical property changes. Exceptions to this observation are yield strength changes, particularly in pure metals, irradiation creep as related to void swelling, and a limited treatment of helium embrittlement. Hence, possible relationships between the critical differences in fission reactor and FFW conditions and mechanical property changes will not be discussed except to note the following:

a. Crude calculations[15] and experimental data[28] suggest that high levels of helium in FFWs will result in more severe reductions in tensile and creep rupture ductility than produced in irradiations to equivalent dpa in fission reactors at temperatures above 500°C.

b. The pulsed irradiation environments of FFW strongly suggest that fatigue and crack growth may be an important limitation on wall lifetimes. Degradation in fatigue properties has often been observed to accompany reductions in ductility. The presence of severe surface damage in FFWs may further exacerbate fatigue and ductility failure problems.

c. Transmutant and impurity hydrogen isotopes may also degrade mechanical properties in FFW.

The authors believe that increased effort on the problem of relating microstructural changes to property changes is essential to a complete damage analysis program. More work is needed on modeling and deriving empirical correlations for the following phenomena: interaction of mobile dislocations with altered microstructure resulting in changes in plastic flow stresses; influence of irradiation induced point defect concentrations and microstructure on time dependent creep deformation mechanisms and local composition; alteration of microscopic failure mechanisms of crack or cavity nucleation; and growth in both the tensile fracture and creep rupture regimes due to damage microstructure. Interactions between various mechanisms--e.g., lattice hardening and grain boundary crack propagation--should be investigated in such studies. Development of microstructural-property change correlations is particularly important in optimizing the information available from neutron sources with small irradiation volumes.

D. SEMI-EMPIRICAL DATA CORRELATION METHODS

Because sound physical models of radiation damage that are widely predictive of experimental results are not available, semi-empirical methods have been developed to synthesize mathematical correlation methods with existing physical information. In addition to providing a nominal correlation of data, these methods can yield systematic estimates of uncertainties in projections of damage response. The implicit comparisons of theory and experiment in these procedures provide clues concerning the underlying mechanisms of radiation damage.

1. Semi-Empirical Damage Function Analysis[29-31]

The damage function analysis (DFA) method assumes that a specified property change P for a specific material exposed in a spectrum $\phi_j(E)$ (normalized to unity) can be expressed as

$$P = (\Phi t)_j \int G_p(E)\, \phi_j(E) dE \qquad j = 1,N \qquad (4)$$

Here $(\Phi t)_j$ is the total fluence required to produce P, and the spectrum weighting function $G_p(E)$ is called the damage function.

The damage function $G_p(E)$ is derived using an iterative computer algorithm to solve the set of N equations. The necessary experimental data are N values of $(\Phi t)_j$ required to produce P in N known spectra $\phi_j(E)$. All other irradiation variables are assumed constant or appropriately corrected to simulate uniform conditions.

The solution begins with an assumed energy dependence $G^\circ(E)$ which should reflect existing knowledge of the damage mechanism. Functions currently used are based on models of displacement type damage or helium production cross sections. The iterative

solution procedure is terminated when differences between calculated and measured P are consistent with experimental uncertainties. The derived $G_p(E)$ can be used to predict fluences needed to produce P in other spectra, provided that other variables are similar or are not significant.

Thus an important feature of DFA is the systematic synthesis of theoretical and experimental information. Another important aspect of DFA is estimation of some uncertainties in $G_p(E)$ and fluences derived from them. Solution uncertainty due to a lack of solution uniqueness and data error propagation is estimated using Monte Carlo methods which involve repeated solutions using data sets and trial solutions randomly varied over appropriate ranges.

Damage functions have been derived for a number of materials and conditions including high temperature and fluence irradiations of stainless steel (SS). Both uniqueness and data error contributions to solution uncertainties are relatively small in energy regions where an appreciable amount of damage is produced in test spectra. Outside these regions uncertainties are large and the accuracy of $G_p(E)$ is primarily dependent on the physical realism of $G°(E)$ and the magnitude of data errors.

A more fundamental question involves the rigorous existence of a damage function. Interactions between unlike defects, strong rate or time history effects, or energy dependence of the damage mechanism invalidate the basic assumption in Equation 4. For example, if damage was the result of a first order interaction between helium and displacement damage, $G_p(E)$ would depend on the spectrum.

There is substantial experimental and theoretical evidence that damage functions effectively exist in many cases. It should

be noted that even if a damage function does not rigorously exist, the DFA correlation procedure may be capable of providing reasonable and conservative damage projections, at least for moderate spectral extrapolation.

Utilization of existing damage functions derived from fission reactor irradiations to project FFW response is uncertain because the lack of significant damage generation above 5 MeV in these environments results in large data and solution uniqueness errors. Existing damage functions based on fission reactor data show an uncertainty of about a factor of 2 when applied to FFW damage projections.[32] However, these results do not include estimates of uncertainty due to the question of damage function existence in FFW situations where, for example, there may be interactive damage phenomena or altered damage mechanisms due to high concentrations of helium.

An analytical study of the effectiveness of various sets of spectral environments for defining damage functions for FFW applications has also been carried out.[32] The spectral sets included some intermediate neutron source spectra. Three damage models were assumed, including two in which the damage function method is rigorously applicable and a third where a damage function independent of spectrum does not exist. In the latter case DFA was found to be ineffective when only fission reactor data were used. The addition of a high energy neutron source, such as 35 MeV (d,n) or 14 MeV ABEs greatly reduces the errors in the DFA correlation method even in the case where a damage function does not rigorously exist.

Although DFA has been primarily used to define the neutron energy dependence of damage, the method can also be applied to deriving the PKA energy dependence of displacement damage. Such an analysis might be usefully carried out on neutron and charged particle data to define a cascade vacancy loop production function.

2. Integral Damage Parameter Analysis

To mitigate some of the problems implicit in DFA, an alternative method of data correlation known as integral damage parameter analysis (IDPA) has been studied. Briefly, IDPA is based on linear and/or nonlinear multivariate regression analysis of damage data using parameters and functional forms suggested by our mechanistic understanding of radiation damage from both theory and experiments. The general advantages of IDPA include: (1) it allows synthesis of experimental and theoretical information in data correlation and projection in the form most consistent with damage mechanisms; (2) it can directly account for interactive effects; (3) a number of damage variables may be analyzed simultaneously, potentially enlarging the available data base; and (4) the mathematical basis of the analysis is firm and uncertainty estimates of statistical and model errors can be made directly.

In addition to the fact that IDPA does not directly provide differential energy dependence information (if indeed it exists), it shares with other correlation methods the following general disadvantages: (1) There is a model sensitivity in terms of correlation functional forms and integral parameters. Even relatively complex functions may not adequately reflect actual damage response, and the damage parameters, as defined quantities, are subject to uncertainty. Fitting physically realistic functions may require larger controlled sets of data than are generally available. (2) The analysis may provide a good mathematical correlation of available data but lack a real physical basis. Hence, correlations may incorrectly predict damage response, particularly where extrapolations are involved. (3) Data errors may propagate and magnify in such an analysis.

The regression form may be linear as

$$\Delta P = \alpha IP_1 + \beta IP_2 + \gamma IP_3 + \ldots \qquad (5)$$

or nonlinear such as, for example,

$$\Delta P = IP_1^{\alpha} + \beta IP_2 \exp(\gamma IP_3). \qquad (6)$$

Integral damage parameters (IP_i) include dpa and displacement rate, helium per atom, helium-to-displacement ratio, temperature, and so on.

A preliminary study of the method has been applied to a limited number of "reasonably" well characterized data sets. Some success has been achieved for the yield stress of austenitic stainless steel and iron and nil-ductility changes in ferritic steels. Analysis of ductility data has not been very fruitful to date but efforts are continuing. However, one study has found a favorable correlation of ductility data for stainless steel irradiated in EBR-II and HFIR using the square root of the product of a total helium times displacements in a functional form incorporating damage saturation.[33] Analysis of helium influence on void swelling is underway, as is testing the method against "complex" model-based calculations in controlled computer simulation experiments. While these very early studies suggest that IDPA is a potentially effective way of correlating irradiation effects data, application will require a much more extensive data base. Furthermore, a maximum of physical guidance in selecting correlation parameters and functional forms is mandatory if mathematical artifacts are to be avoided.

E. SUMMARY

The set of currently available irradiation environments and correlation procedures is not a sufficient basis for confident quantitative FFW damage projections. The high energy neutron environments from the (d,n) ABEs will be very useful in establishing damage behavior under more realistic FFW conditions than found in fission reactors. Optional utilization of this information depends on developing generalized correlation procedures, physically sound damage models, and accurate damage parameter definition. A semi-empirical correlation method which uses integral damage parameters in a regression type analysis is one promising approach.

However, physical models of damage response must be developed to, at the minimum, provide guidance and a conceptual framework for designing experiments and correlation efforts. It should be clear from this discussion that a quantitatively predictive comprehensive model is not near at hand. Although the defect production exposure parameters are in fairly good shape for neutrons below 15 MeV, uncertainties are potentially large above this energy. This is also the case for neutron dosimetry. On the other hand, absolute calculations of particular displacement defect types are subject to greater errors due to uncertainties in secondary defect production models. Models of microstructural evolution and property changes are currently only qualitatively description. The authors believe that significant improvements can be achieved.

In view of the current state of ignorance and the potential complexity of damage phenomena in FFWs, a vigorous program of comprehensive damage analysis development is clearly needed. Ad hoc, highly empirical stabs at correlating and projecting data are not likely to be productive. The prospect is to have only a limited number of test environments, none of which are ideal. Damage analysis tools must be developed to optimize the usefulness of this set of diverse environments.

Although much of the discussion in this report of radiation-induced microstructures has dealt with the effects of helium on swelling, this is not meant to imply that swelling is expected to be the dominant FFW phenomenon. Rather, substantial collective evidence suggests that changes in mechanical properties will be more significant in limiting FFW lifetimes. In this regard, control over the distribution of helium may be important in the development of radiation resistant alloys. This illustrates the importance of gaining a fundamental understanding of damage mechanisms.

F. ACKNOWLEDGMENT

The authors gratefully acknowledge helpful discussions of the ideas presented in this report with A. N. Goland, L. R. Greenwood, C. M. Logan, D. M. Parkin, T. C. Reuther, Jr., M. T. Robinson, and J. O. Stiegler, fellow members of an ad hoc ERDA Damage Assessment Panel.

G. REFERENCES

1. Proceedings of the International Conference on Radiation Test Facilities for the CTR Surface and Materials Program, ANL/CTR-75-4, July (1975).

2. See special issue of Nucl. Tech. 25, 169-492 (1975).

3. G. R. Odette, Trans. ANS 22, 803 (1975).

4. A recent review of radiation damage research as applied to fusion technology is Radiation Effects and Tritium Technology for Fusion Reactors, J. S. Watson and F. W. Wiffen, eds., CONF-750989, March, 1976.

5. G. R. Odette and D. R. Doiran, Nucl. Tech. 29-3, 346 (1976).

6. F. W. Wiffen and J. O. Stiegler, "Recent Progress in CTR Bulk Radiation Effects Studies," this volume.

7. E. P. Lippincott, W. N. McElroy, and H. Farrar, IV, Nuclear Cross Sections and Technology, NBS-425 1, 375 (1975).

G. REFERENCES (Cont'd)

8. A good review of rate theory of void swelling is found in A. Bement, Adv. Nucl. Sci. Tech. 7, 1 (1973). See also the Proceedings of the Consultant Symposium on The Physics of Irradiation Produced Voids, R. S. Nelson, ed., AERE-R7934, January 1975, and references cited therein.

9. J. F. Westmoreland, J. A. Sprague, F. Smidt, and P. Malmberg, Rad. Effects 26, 1 (1975).

10. G. R. Odette and R. Myers in Controlled Thermonuclear Research Quarterly Progress Report, HEDL-TME 75-90, July 1975, p. 2.

11. J. O. Schiffgens, D. G. Doran, and N. J. Graves, See Reference 4 above, p. I-532.

12. R. Bullough, B. L. Eyre, and K. Krishan, Proc. Roy Soc. A 346, 81-102 (1975).

13. G. R. Odette and S. R. Schwartz, in Controlled Thermonuclear Research Quarterly Progress Report, HEDL-TME 75-24, February 1975, p. 17.

14. K. C. Russell and D. H. Hall in Defect and Defect Clusters in BCC Metals and Their Alloys, R. J. Arsenault, ed., AIME Nucl. Metall. 18, 545 (1973).

15. G. R. Odette and M. W. Frei in Proc. of First Topical Meeting on the Technology of Controlled Nuclear Fusion, G. R. Hopkins, ed., CONF-740402-P2, April, 1974, p. 485.

16. G. R. Odette and S. L. Langley, See Reference 4, p. I-395.

17. R. Bullough and M. R. Haynes, See Reference 4, P. I-230.

18. F. Smidt and A. Pieper, See Reference 4, p. II-280.

19. H. Wiedersich, J. Burton, and J. Katz, Journ. Nucl. Mat., 51 287 (1974).

20. G. W. Greenwood, A. J. E. Foreman and D. E. Rimmer, Journ. of Nucl. Mat. 4, 305 (1959).

21. A. Brailsford and R. Bullough, Journ. of Nucl. Mat. 48, 87 (1973).

22. A. T. Santhanam, A. Taylor, and S. D. Harkness, in Defects and Defect Clusters in BCC Metals and Their Alloys, R. J. Arsenault, ed., AIME Nucl. Metall. 18, 302 (1973).

G. REFERENCES (Cont'd)

23. D. J. Mazey and R. S. Nelson, See Reference 4, p. I-240.

24. J. Brimhall and E. Simonen, Trans ANS, 22-1, 176 (1975).

25. J. Brimhall and E. Simonen, BNWL-1939-2, 36 (1976).

26. K. Farrell and J. Houston, See Reference 4, p. II-209.

27. P. J. Maziasz, F. W. Wiffen, and E. E. Bloom, See Reference 4, p. I-259.

28. F. W. Wiffen and E. E. Bloom, Nucl. Tech. 25, 113 (1975).

29. R. L. Simons and G. R. Odette, "Damage Analysis: Damage Function Development and Application," HEDL-SA 917, Sept. 1975.

30. G. R. Odette, R. L. Simons and W. M. McElroy, "Reactor Materials Performance Predictions Using Damage Functions: Analysis of Fluence Limit Uncertainties," HEDL-TME 75-43 (1976).

31. D. G. Doran, R. L. Simons, and G. R. Odette, "Damage Function Analysis for Fusion Reactor Applications," HEDL-SA 876, April 1976.

32. R. L. Simons and D. G. Doran, See Reference 4, p. II-18.

33. R. L. Simons, "Neutron Energy Dependent Damage Functions for Tensile Properties of 20% C.W. 316 Stainless Steel," HEDL-SA 1057, April 1976.

TASK GROUP ON DAMAGE ANALYSIS AND FUNDAMENTAL STUDIES (DAFS)

D. G. Doran/W. M. McElroy (HEDL)

The objective of this Task Group is the development of procedures and supporting technology for the application to fusion reactor design environments of data on property changes of materials obtained in neutron and charged-particle test environments. The scope includes:

- development of procedures for characterizing neutron environments of test facilities and fusion reactors;
- theoretical and experimental investigations of the influence of irradiation environment on damage production, damage microstructure evolution, and mechanical and physical property changes;
- and identification of need for, and, where appropriate, development of essential nuclear and materials data.

The initial membership of the task group has been selected and an organizational meeting was held on October 7-8, 1976 at Germantown. Five subtasks have been identified. The membership and their initial subtask assignments are shown in Table 1. The short-term schedule adopted by the task group, in order to have a draft version of a long-range program prepared by April 1, 1977 is given in Table 2. Problem analyses have been prepared by the subtask groups for discussion at the task group meeting scheduled for January 18-19, 1977 at Los Alamos.

IV. EXPECTED ACCOMPLISHMENTS

Analysis of the low energy displacement cascades is continuing. A more complete description of the defect configurations is in preparation. A draft of a document describing SCAS is currently being prepared for comments. The next step will be to begin processing cascades with SCAS using different sets of parameters in order to determine optimum means of application to real cascades and to obtain data for comparison with previous results obtained with HAPFCC.

TABLE 1

MEMBERSHIP OF DAFS TASK GROUP AND SUBTASK ASSIGNMENTS

Member	Subtask[a] A	B	C	D	E
D. G. Doran (Chairman), HEDL	e-o[b]	e-o	e-o	e-o	e-o
H. Farrar, IV, AI	m				
A. N. Goland, BNL	m	m			
R. R. Heinrich, ANL	c				
F. V. Nolfi, ANL					c
G. R. Odette, UCSB			c		
D. M. Parkin, LASL	m	m			
T. C. Reuther, Jr., US-ERDA	e-o	e-o	e-o	e-o	e-o
M. T. Robinson, ORNL		c			
F. A. Smidt, Jr., NRL			m	m	m
R. R. Vandervoort, LLL			m	c	m
P. Wilkes, U of Wisconsin			m		

[a] Subtasks are:

A. Environmental Characterization
B. Damage Production
C. Damage Microstructure Evolution
D. Mechanical Behavior
E. Joint Subtask with Task Group on Alloy Development and Irradiation Performance

[b] e-o = Ex-officio member
m = Member
c = Chairman

TABLE 2

SCHEDULE OF TASK GROUP AND SUB-TASK GROUP ACTIVITIES

October 15, 1976	Scope and objectives statements of the Sub-Task Groups sent to Task Group Secretary (A. N. Goland) for distribution to members.
October 31, 1976	Sub-Task Group membership recruitment completed.
December 20, 1976	Sub-Task Groups complete problem analysis and propose approach to solution (identify capabilities needed, relationship to other Sub-Task Groups, etc.).
January 18-19, 1977	Task Group meets to review work of Sub-Task Groups (at LASL).
January 24, 1977	Comments of Task Group distributed to Sub-Task Groups.
February 28, 1977	Final drafts of Sub-Task Group reports sent to Task Group members (includes milestones, manpower needs, priorities, etc.).
March 16-17, 1977	Final review by Task Group (at U.C.-Santa Barbara).
April 1, 1977	Draft report of Task Group to DMFE Materials Branch.

The Task Group on Damage Analysis and Fundamental Studies will hold its second meeting at Los Alamos on January 18-19, 1977. The primary purpose of the meeting will be discussion of problem analyses prepared by the sub-tasks and planning for the next activity, which is program definition.

V. COMMUNICATIONS AND MEETINGS

- D. G. Doran participated in the initial meeting of the ERDA-DMFE Fusion Materials Coordinating Committee on December 9-10, 1976 at Germantown.

- D. G. Doran participated in an IAEA Specialists Meeting on Radiation Damage Units at Harwell, United Kingdom, November 2-3, 1976.

- D. G. Doran participated in the US-USSR Exchange on Fusion Materials: Bulk Irradiation Effects at Moscow, November 10-23, 1976.

VI. REPORTS AND PUBLICATIONS

- J. O. Schiffgens and R. D. Bourquin, "Computer Simulations of Low Energy Displacement Cascades in a Face Centered Cubic Lattice", HEDL-SA 886, submitted to the International Conference on the Properties of Atomic Defects in Metals, Argonne National Laboratory, October 18-22, 1976.

- D. G. Doran and G. R. Odette, "Radiation Damage Analysis as Applied to Fusion Reactor First Walls", to appear in proceedings of ANS meeting on "The Technology of Controlled Nuclear Fusion" held in Richland, WA, September 21-23, 1976.

- D. G. Doran, D. M. Parkin, and M. T. Robinson, "Damage Energy and Displacement Cross Sections: Survey and Sensitivity", to be published in IAEA technical report of a Specialists' Meeting on Radiation Damage Units, Harwell, UK, November 1976.

MECHANICAL PERFORMANCE OF MFE MATERIALS (ED-02-03 EDB)

MECHANICAL PERFORMANCE OF MFE MATERIALS

E. K. Opperman and J. L. Straalsund (HEDL)

I. OBJECTIVE

The objective of this program is to establish the effects of Magnetic Fusion Reactor (MFR) environments on the mechanical properties of candidate MFR materials. As a first step in meeting this end, a torsional system was developed[1] to measure creep resulting from incident light ions of energies ranging from 5 to 60 MeV and displacement rates up to 1×10^{-5} dpa/sec. Light particle simulation of creep and cyclic behavior will be necessary during early stages of MFR materials development because high flux neutron sources will not be available during this period.

The specific objectives of this six month period were to finalize the thermal creep testing phase and initiate creep measurements under proton irradiation. The goals of the first irradiation were to determine if proton induced creep could, in fact, be resolved from thermal creep and to give the entire system, including all beam defining, collimating and measurement components, a thorough test in a radiation environment.

II. SUMMARY

A torsional creep testing machine is being developed to be used in conjunction with an accelerator for the purpose of determining the phenomenology and alloy dependence of atomic displacement enhanced creep. Initial development and thermal testing of the creep rig are described in an earlier report[1].

This report describes the first irradiation test. The test was performed on 20% cold worked Type 316 stainless steel and involved the use of the 30-inch cyclotron at the Lawrence Livermore Laboratory. This machine is capable of accelerating protons to 14.8 MeV with beam densities of $\sim 15 \mu A/cm^2$, which corresponds to a displacement rate of about 5×10^{-7} dpa/sec.

The test was conducted over a period of 600 hours and involved the use of about 130 hours of beam time. The first stage of the experiment was a thermal creep test, about 150 hours in duration. Subsequent portions of the test involved "beam on" periods ranging from 5 to 40 hours with displacement rates up to $\sim 4 \times 10^{-7}$ dpa/sec and "beam off" periods during which the temperature and stress were maintained essentially constant. The creep rates observed during "beam on" conditions were over an order of magnitude larger than that observed during "beam off" conditions. Daily variations in beam density provided data from which correlations between creep rate and flux density were obtained.

III. ACCOMPLISHMENTS AND STATUS

A torsional creep testing machine is being developed to be used in conjunction with an accelerator for the purpose of determining the phenomenology and alloy dependence of atomic displacement enhanced creep. Initial development and thermal tests of the creep rig are described in an earlier report[1] whereas this report describes the first accelerator irradiation test which was performed on 20% cold worked steel using the 30-inch cyclotron at the Lawrence Livermore Laboratory.

The general experimental arrangement has been discussed earlier[1] and is summarized in Figures 1-4. Figure 1 shows the load train which consists of an electro-magnetic coil which applies torque to the small diameter .127 mm wire specimen. Strain is monitored by an electro-optical rotation gage which tracks the rotation of a mirror mounted on the bottom of the coil. The location of this gage is shown in Figure 2 which also shows the helium gas loop which is used to control specimen temperature. The helium velocity in the vicinity of the specimen is very high, on the order of 10^4 cm/sec, which minimizes the difference in temperature between specimen and the gas stream. The temperature of the gas stream is controlled by the heater which is capable of providing gas temperatures to 540°C. The creep system is connected to the accelerator so that the proton beam is perpendicular to the helium gas stream as shown in Figure 3.

Figure 4 is a top view of the specimen chamber illustrating the relative locations of the gas inlet and outlet jets and the proton beam collimator.

Beam Diagnostics

Three independent means of beam density measurements were used. The first technique simply consisted of measuring the total beam current passing through a collimator of known area. A second indication of the beam intensity was obtained by monitoring the temperature difference between a thermocouple located right next to the actual specimen (Fig. 5) and the helium gas stream. This thermocouple had the same mass and aerodynamic characteristics as the specimen and therefore experienced beam heating very similar to that of the specimen. Thus the measurement of the thermocouple ΔT gave an indication of the beam intensity at that point. Measured ΔT's ranged from 15 to 30°C. The third means of determining a measure of the beam density is through post irradiation gamma ray spectroscopy. When calibration of this technique is complete, it will yield a measure of the integrated beam profile (axial) and total dose.

Specimens

The specimen for this initial test was obtained from a particular heat of stainless steel which has been used extensively in LMFBR studies (Heat 87210) and was fabricated by drawing with the final pass consisting of a 20% reduction of area resulting in 0.76 mm diameter wire. The wire was cut to approximately 7.5 cm length and the central $\sim$1.5 cm length was chemically polished. This method of fabrication resulted in a gradually tapering gage length as shown in Figure 6. As a result of chemical polishing, the variation of diameter with axial position must be accurately known in order to calculate parameters such as proton energy deposition, shear stress, displacement rates, and so forth. In this experiment, diameter measurements were obtained through the use of 30X photographs of the specimen gage lengths.

Temperature Control

Previously, it had been planned to provide temperature control by actively controlling the temperature of the control thermocouples located next to the specimen shown in Figure 5. While this technique follows gradual 10-20% variations in the beam, it lacks the quick response time necessary to follow rapid changes in the beam density. Thus, in order to avoid the possibility of overheating the specimens during transient beam on/off periods, the gas temperature was controlled by a thermocouple upstream of the beam and maintained at a temperature $\sim$20°C below the nominal specimen operating temperature (400°C). In this manner, the specimen temperature became $\sim$400°C during the periods of time when the beam was on and dropped to $\sim$380°C during short periods when the beam was off. After the daily 16-hour irradiations, the gas temperature was again returned to 400°C for the 8-hour beam off period, thus keeping the average specimen temperature less than or equal to 400°C.

Stress Strain Relationships

The present experiment involves torsion of a solid rod and therefore a varying stress field. In the temperature range explored, irradiation creep rates have usually been observed to be linearly dependent upon stress. This assumption is implicit in the following discussion which describes the relationships which were used to calculate stress and strain from the experimental variables.

To compare the shear strain rates with the more commonly cited uniaxial rates, the following relation[2] was used:

$$\frac{\gamma}{3\tau} = \frac{\varepsilon}{\sigma} \qquad (1)$$

where γ = shear strain, τ = shear stress, ε = uniaxial strain, and σ = uniaxial stress. Shear strain (γ) is a function of effective radius (r_e), angle (θ) through which the specimen rotates, and the active gage length (L_e).

$$\gamma = \frac{r_e \theta}{L_e} \qquad (2)$$

The criteria chosen for determing the active gage length is the distance between diameters (D, Figure 7) such that the stress at those diameters is one fourth the maximum stress placed on the specimen.

Since the radius is gradually varying over the active gage length of the specimen, one must also derive an effective radius. This effective radius is determined from the measured elastic properties of the specimen prior to irradiation. The specimen radius or effective radius (r_e) in this case, is related to the shear modulus G, the active specimen length L_e, and the slope (m) of the torque (τ) versus rotation (θ) curve, in the following way[2]:

$$r_e = \left[\frac{2L_e\, m}{\pi G}\right]^{1/4} \qquad (3)$$

where $m = \Delta\tau/\Delta\theta$. The specimen is thus described by an active length and effective radius. The calculated stress (τ) in Equation 1 is based on the effective radius of the specimen,

$$\tau = \frac{2}{\pi\, r_e^{\,3}}\, \Gamma \qquad (4)$$

and the applied torque Γ.

IV. RESULTS

Creep results obtained from the first test are summarized in Figure 8, which illustrates the temperature and stress corrected strain-time relation for the entire 600 hour experiment. Irradiation creep was easily resolved as the areas of steep slope, with the intermittent plateaus occurring during the beam off condition. The various slopes or creep rates were found to be proportional to daily variations in proton beam density (Figure 9). If one combines the "beam on" portions of Figure 8, normalized to a given flux density, an irradiation creep curve (Figure 10) is obtained expressing strain

as a function of time or dose. Two interesting features illustrated by this data are the presence of an initial transient period and the increased strain rate as a function of dose. This particular functional dependence on dose is also common to fast reactor irradiation creep data[3].

The remaining data relates the correlation of creep rate, current density, and measured ΔT, a quantity proportional to current density. To relate these quantities, a clarification between beam density as measured by the Faraday Cup and beam density as measured by the in beam thermocouples is necessary. A problem in beam focusing, which is thought to have resulted from a helium leak into the accelerator, caused two distinct beam density regimes. During the first three days of irradiation, relatively high ΔT's were measured for a given cup current (Figure 11). Following repair of an O-ring seal in the beam window, the measured ΔT for the same current was reduced by $\sim$50%. The reason for the discrepancy is believed to be a helium leak induced focusing problem which resulted in portions of the beam initially missing the Faraday Cup. Therefore, uncertainties ($\sim$50%) exist in the absolute and relative values of the current density, as measured by the Faraday Cup.

Local beam density calculations in this experiment have thus been based on the measured temperature difference between the thermocouple and cooling gas. This method offers an excellent relative measure of beam density, but the accuracy of the absolute value is primarily limited by the knowledge of the heat transfer coefficient (h) between the cooling gas and the specimen. The relation between beam density, ΔT and h is Newton's Law of Cooling[4]

$$Q = h\ a\ \Delta T \qquad (5)$$

where Q = energy deposited in specimen by the proton beam (watts), h = heat transfer coefficient between flowing helium gas and specimen (watts/cm^2-°C), ΔT = temperature difference between specimen and helium gas, and A = cooling area of specimen. Absolute beam densities are therefore known as accurately as the parameters Q ($\pm$ 15%) and h within a factor of 2.

Assuming linear stress and flux dependencies one can compare data from this experiment with that of other irradiation creep studies carried out at various stresses and displacement rates. Such comparisons have been made and are compiled in Table I. The results obtained by Harwell[5,6] (321 SS) are in agreement with the HEDL proton results, even though many experimental parameters were different.

If one compares the proton irradiation creep rates obtained by HEDL and Harwell with the EBR-II irradiation creep rates it is seen that per dpa, the protons are roughly an order of magnitude more effective in producing creep. This effect is also found in the area of swelling. Protons have been found to produce much higher swelling values than comparable neutron, or heavy ion doses[7]. If this effect can be linearly combined with the calculated displacement rate, one can conceivably obtain effective damage rates on the order of 1 to 5 dpa/day using protons from existing accelerators.

V. CONCLUSIONS

The creep system was tested under irradiation conditions and performance was found to be satisfactory. However, as a result of this first test, a number of areas have been identified where minor modifications will result in significant improvement in performance. These areas include modifications to the beam diagnostics and collimating systems, the data acquisition system, and the temperature control system.

Proton irradiation induced creep was measured and found to be linearily dependent upon the incident flux density. The strain rates were found to increase slightly with fluence in a manner similar to that observed in past fission reactor irradiation creep experiments. Irradiation creep rates, however, were found to be approximately an order of magnitude higher than that observed in the fast fission reactor experiment when compared on a dpa basis. These results appear to be in agreement with similar observations made upon the void formation phenomena in different irradiation environments.

TABLE 1

COMPARISON OF STEADY-STATE IRRADIATION CREEP RATES

Experimenter/ Reference	Type	Energy MeV	Displacement Rate ($\dot{N}$) (dpa/sec)x10^6	Material/ % Coldwork	Temperature °C	Stress (σ) MPa*	Strain Rate ($\dot{E}$) cM/cM-hRx10^6	Normalized Strain Rate ($\dot{E}/\sigma\dot{N}$)x10^2
HEDL/5	Neutron	>.1(EBR-II)	~0.7	316 SS/20%	~427	138	.43	.44
HEDL	Protons	14.8	$0.4(^{+.3}_{-.1})$	316 SS/20%	400	138**	1.8**	3.3**
Harwell/8	Protons	4.0	1.2	321 SS/60%	500	150	7.8	4.3
	Protons	4.0	1.2	321 SS/20%	500	70	3.2	3.8
Harwell/7	Protons	4.0	.7	Nickel	500	125	25.0	28.6
NRL/10	Deuterons	22.0	.135	Nickel	224	345	27.0	58.0

* 1 Ksi - 6.895 MPa

** Torsion values converted to uniaxial.

VI. EXPECTED ACCOMPLISHMENTS

Experienced gained during the initial irradiation has led to a number of design improvements to be incorporated into the system. Improved temperature control and resolution will enable use of significantly higher beam densities, making possible damage rates on the order of 0.4 dpa/day. Improvement in data acquisition and handling will significantly reduce the time required to reduce data and will also provide key information during the course of the irradiations.

Possible areas of investigation for subsequent irradiations include parameter variation such as temperature, stress magnitude and direction, flux, cyclic variation of parameters with time, and finally the study of various alloys and refractories. The latter will be pursued during the next few irradiations, with the primary objective being the measurement of irradiation creep in approximately four different metals. Candidate metals will include alloys such as PE16, stainless steel, and a pure refractory such as molybdenum.

VII. COMMUNICATIONS AND MEETINGS

None

VIII. REPORTS AND PUBLICATIONS

None

IX. REFERENCES

1. E. K. Opperman, H. H. Hirano, and J. L. Straalsund, "Magnetic Fusion Energy Progress Report," HEDL-TME 76-83, September 1976.

2. G. E. Dieter, Mechanical Metallurgy, McGraw-Hill, New York (1961).

3. E. R. Gilbert, J. L. Straalsund, and G. L. Wire, "Irradiation Creep Data in Support of LMFBR Core Design," HEDL-SA-835, April 1976.

IX. REFERENCES (Cont'd)

4. M. M. El-Wakil, Nuclear Heat Transport, International Textbook Company, Scrawton, PA, 1961.

5. R. J. McElroy, J. A. Hudson and R. S. Nelson, "Irradiation Creep During 4 MeV Proton Irradiation," Proceeding of the International Conference held at Gatlinburg, TN, October 1-3, 1975.

6. R. J. McElroy, J. A. Hudson and R. S. Nelson, International Colloquium. Measurement of Irradiation Enhanced Creep in Nuclear Materials. Petten, May 5-7, 1976.

7. D. W. Keefer, Radiation Effects, 24, p. 29, 1975.

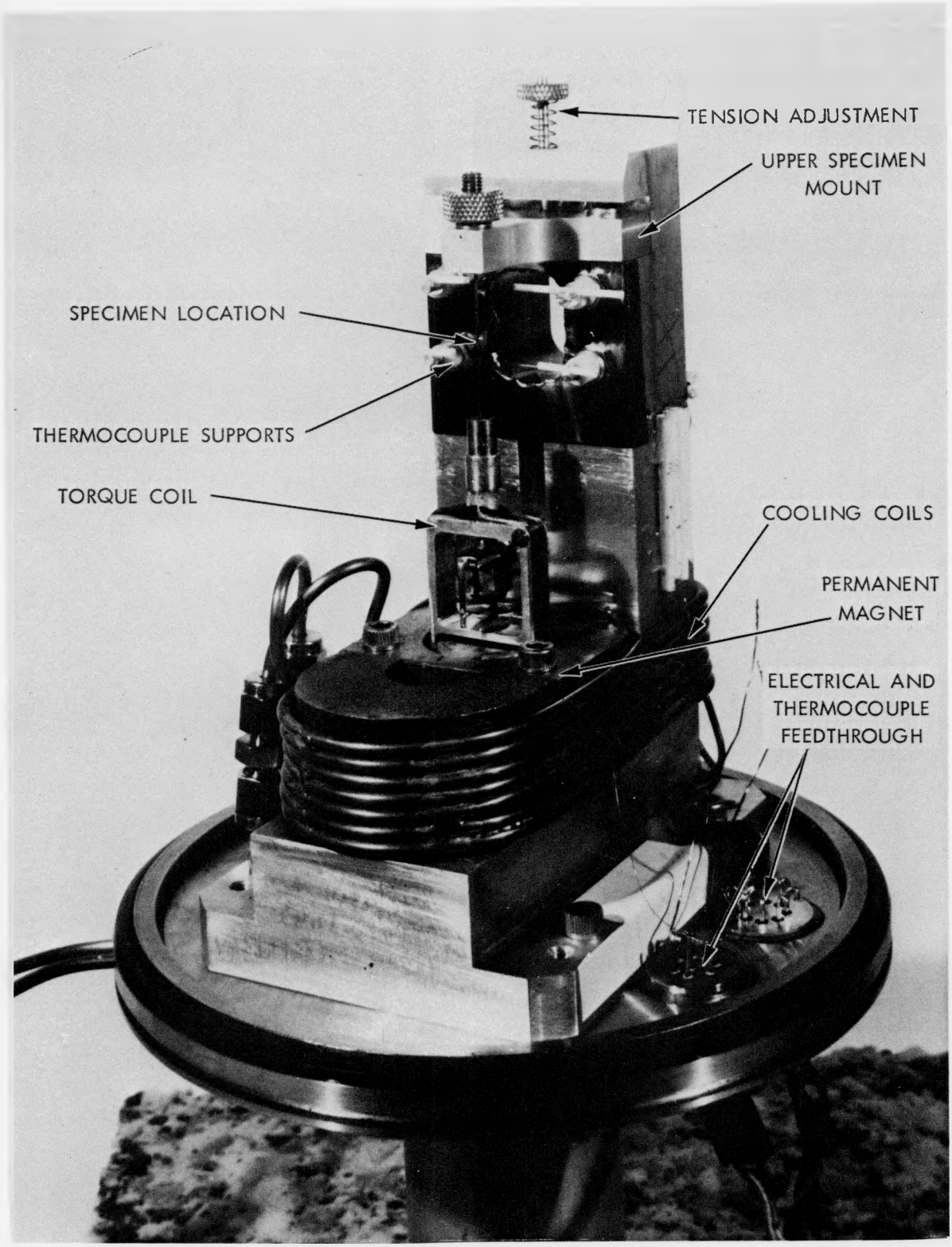

FIGURE 1. Torsional Loading Train. 7611857-3

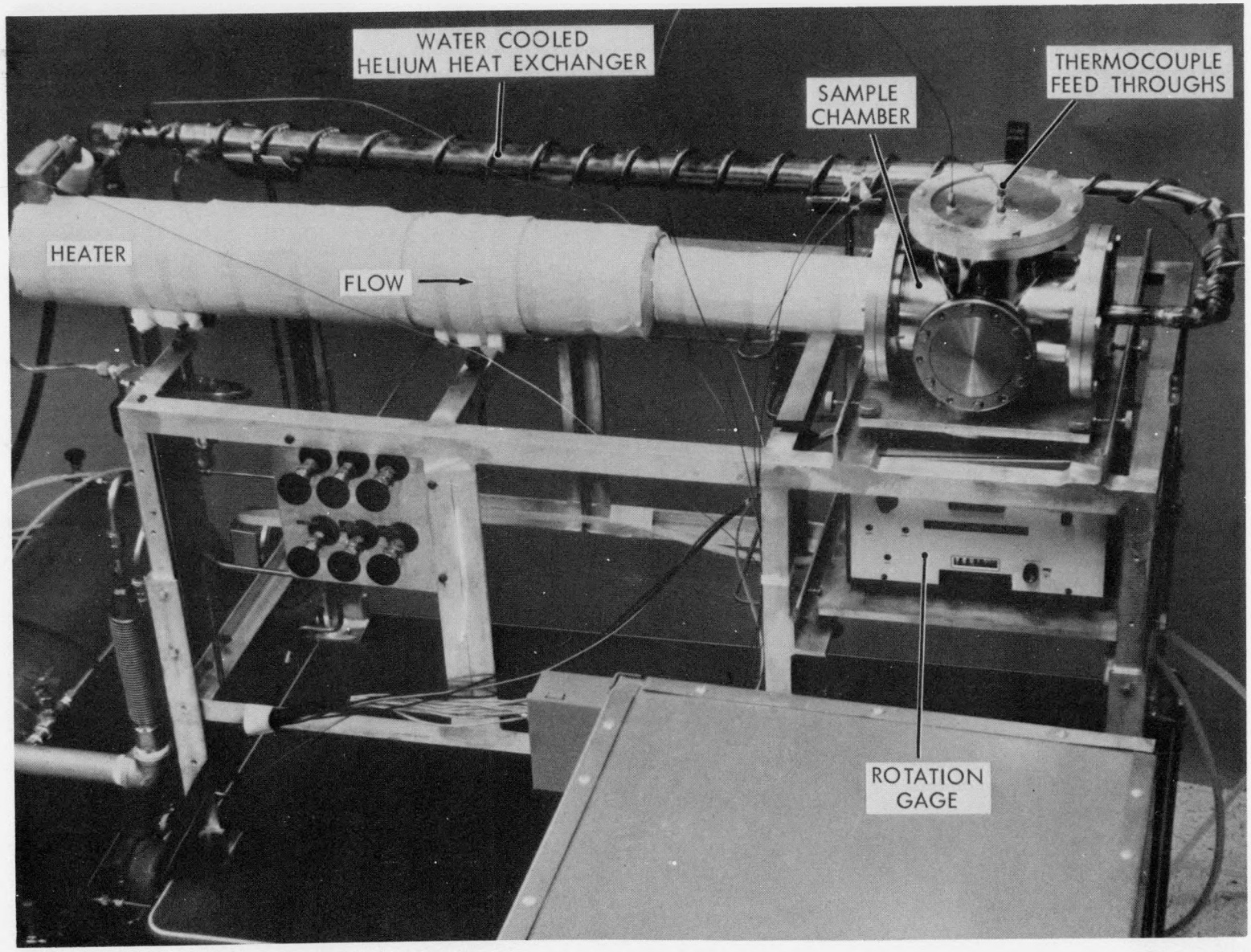

FIGURE 2. Specimen Chamber Stand With Heating and Cooling Legs. 7611660-1CN

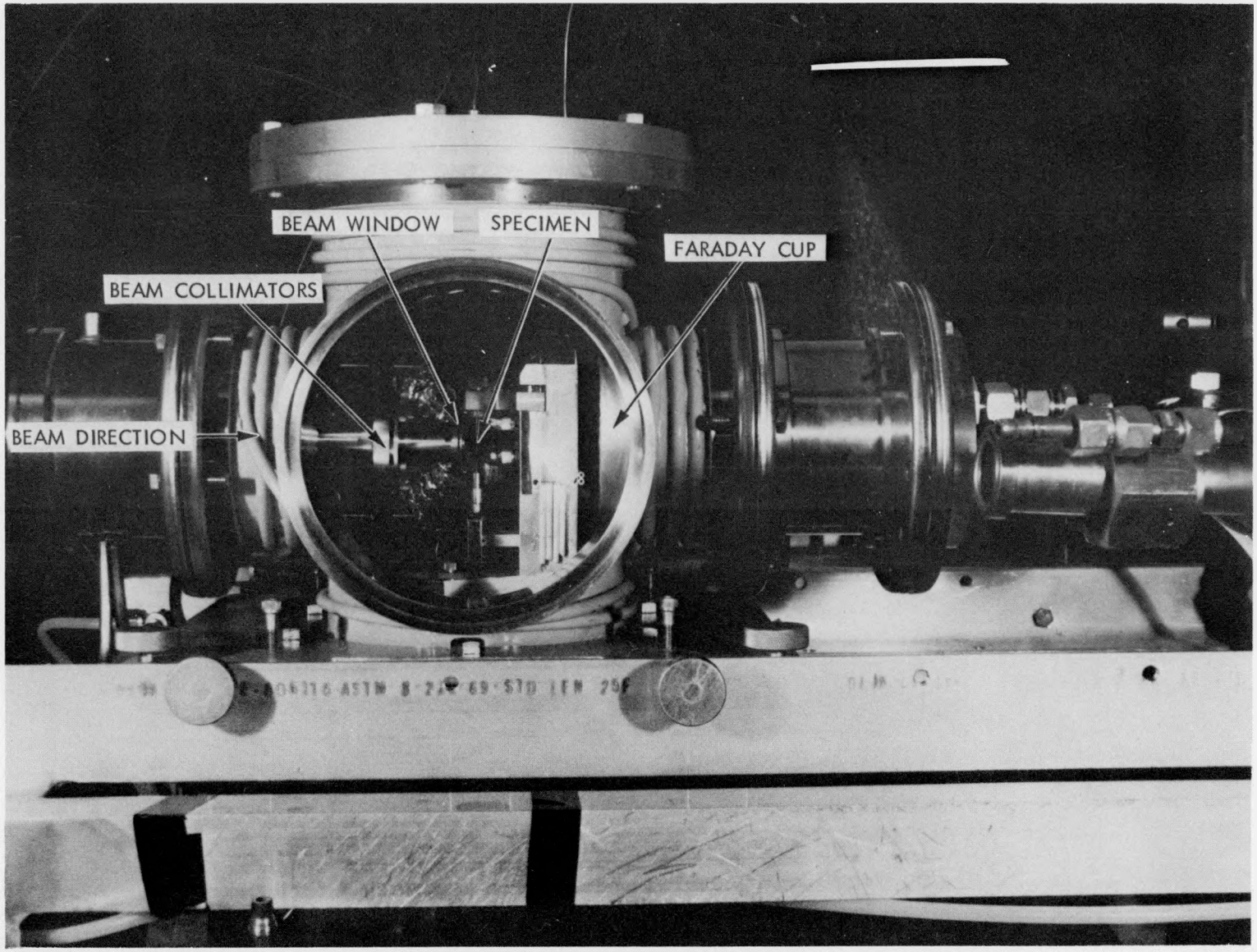

FIGURE 3. View of Specimen Chamber Showing the Proton Entrance and Window Regions. 7611857-2

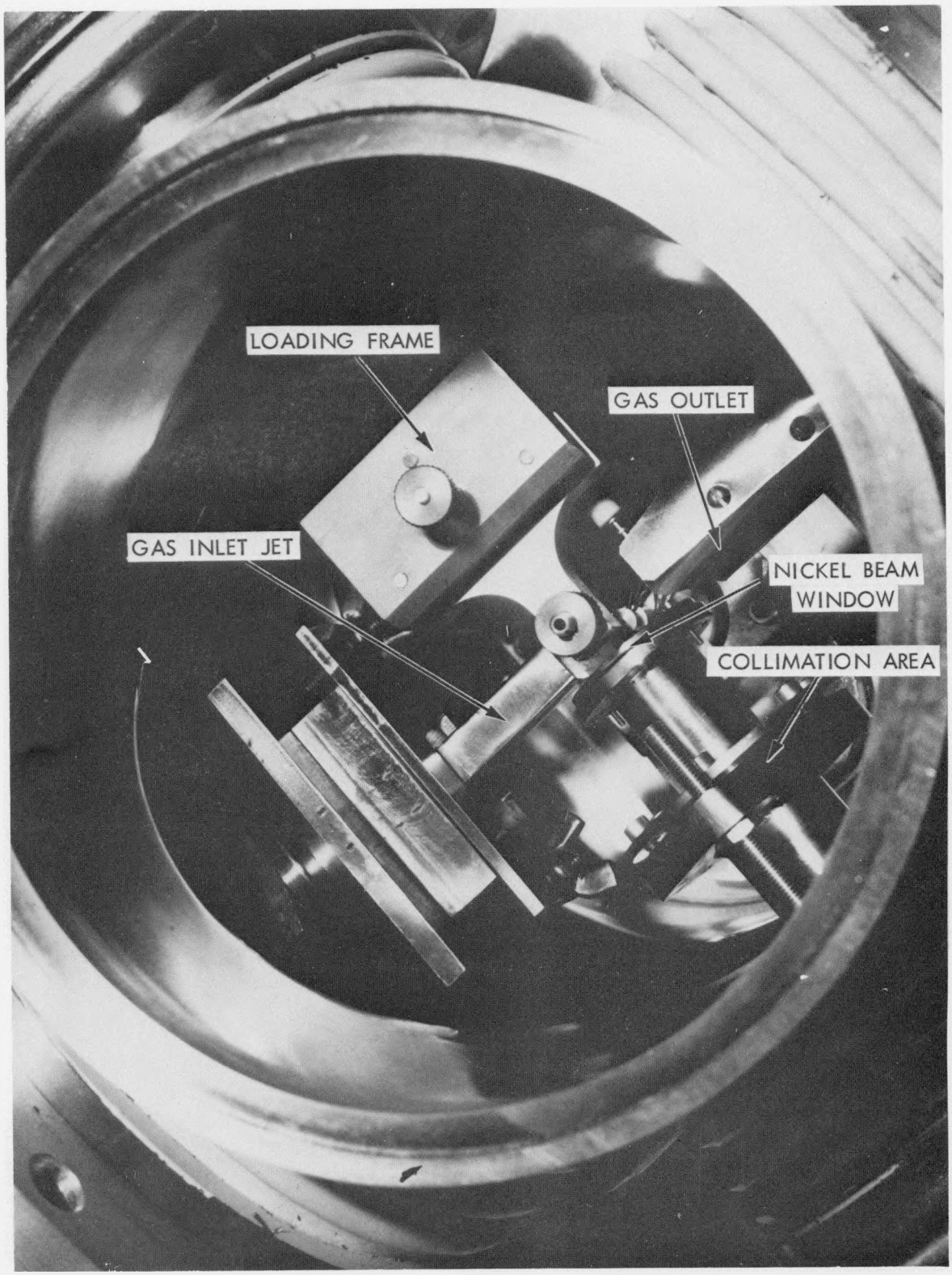

FIGURE 4. Top View of Specimen Chamber. 770106-2

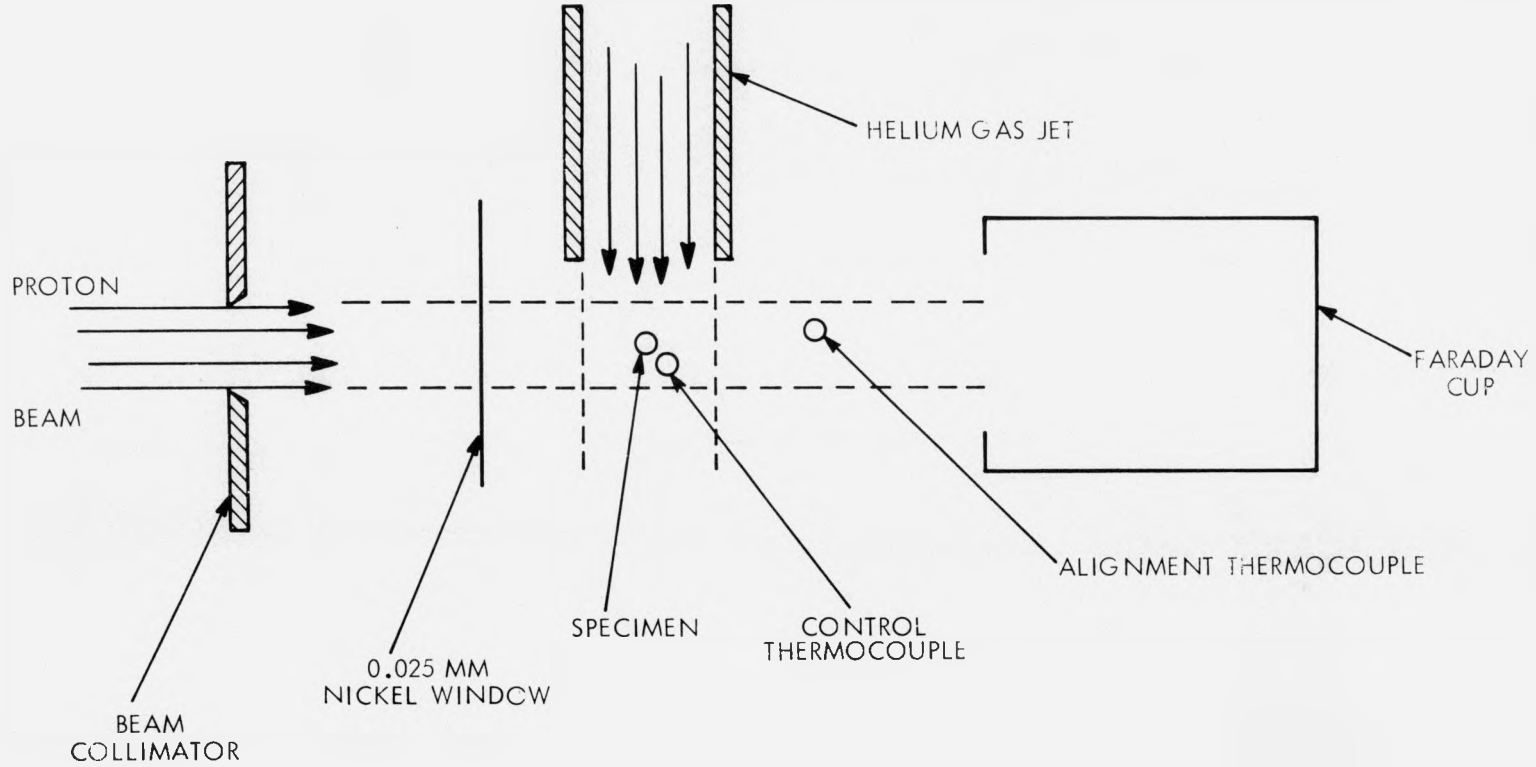

FIGURE 5. Relative Location of Critical Elements Within the Specimen Chamber. HEDL 7612-70.2

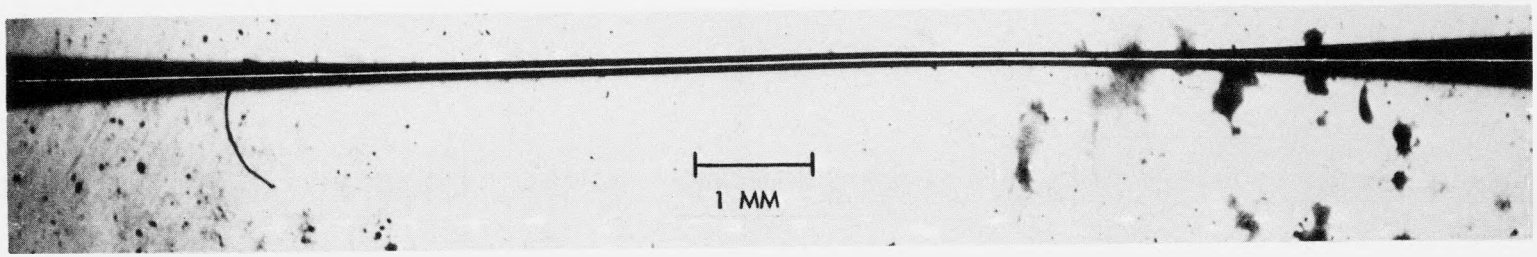

FIGURE 6. 316 Stainless Steel with Minimum Diameter of .14 mm.

7611857-1

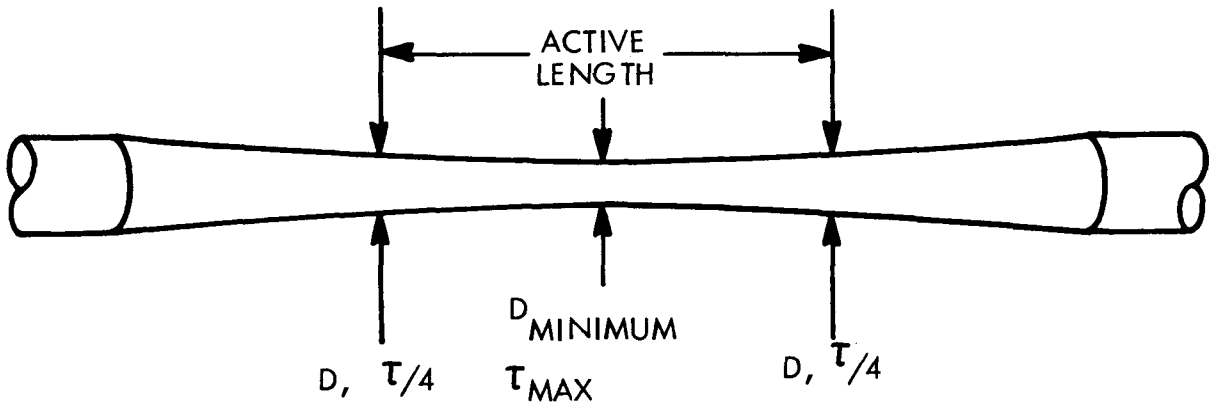

HEDL 7612-70.1

FIGURE 7. Illustration of "Active Length", Where D Is The Diameter and τ Is The Shear Stress.

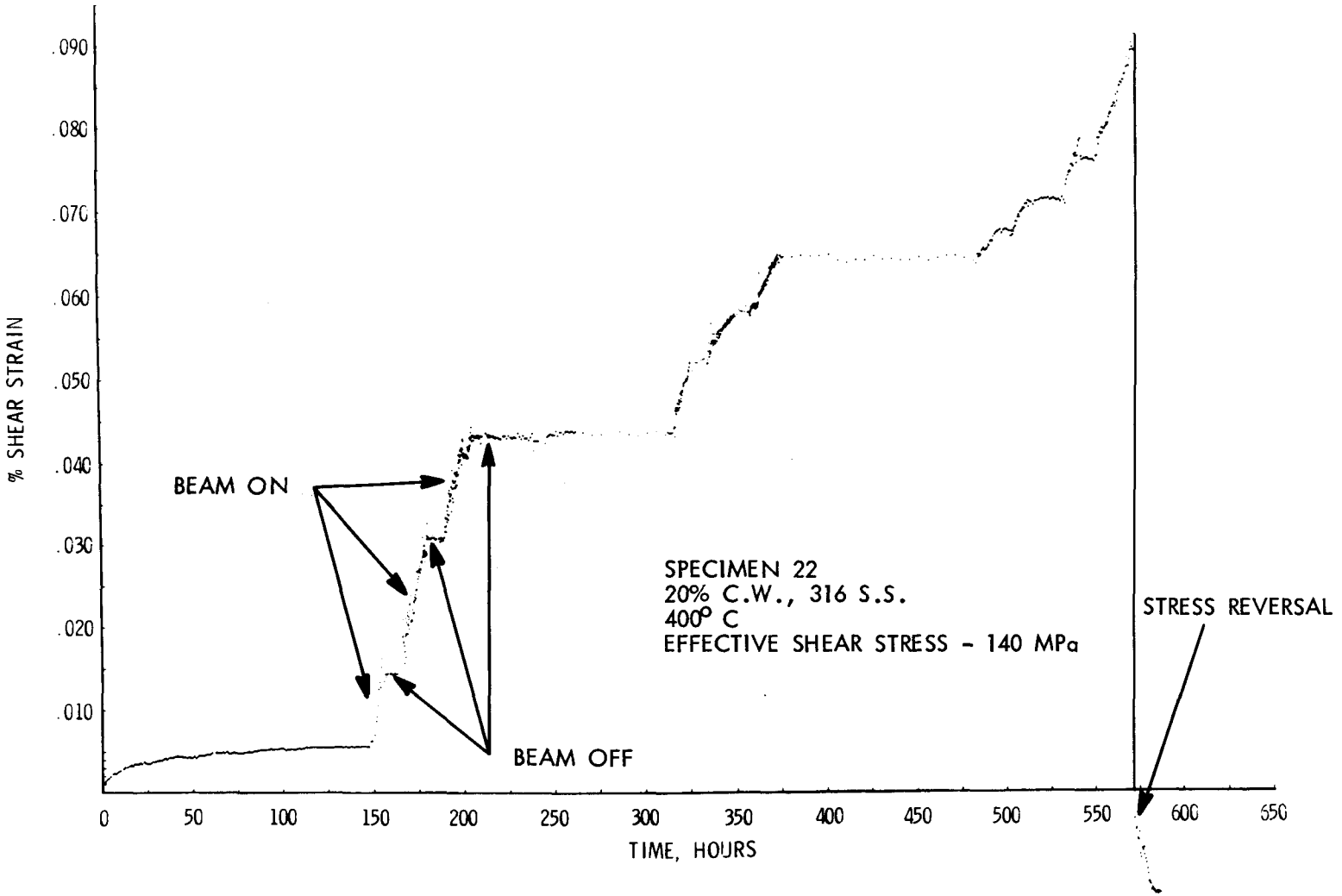

FIGURE 8. Shear Strain Versus Time Illustrating the Significant Difference Between Beam On and Beam Off Conditions.

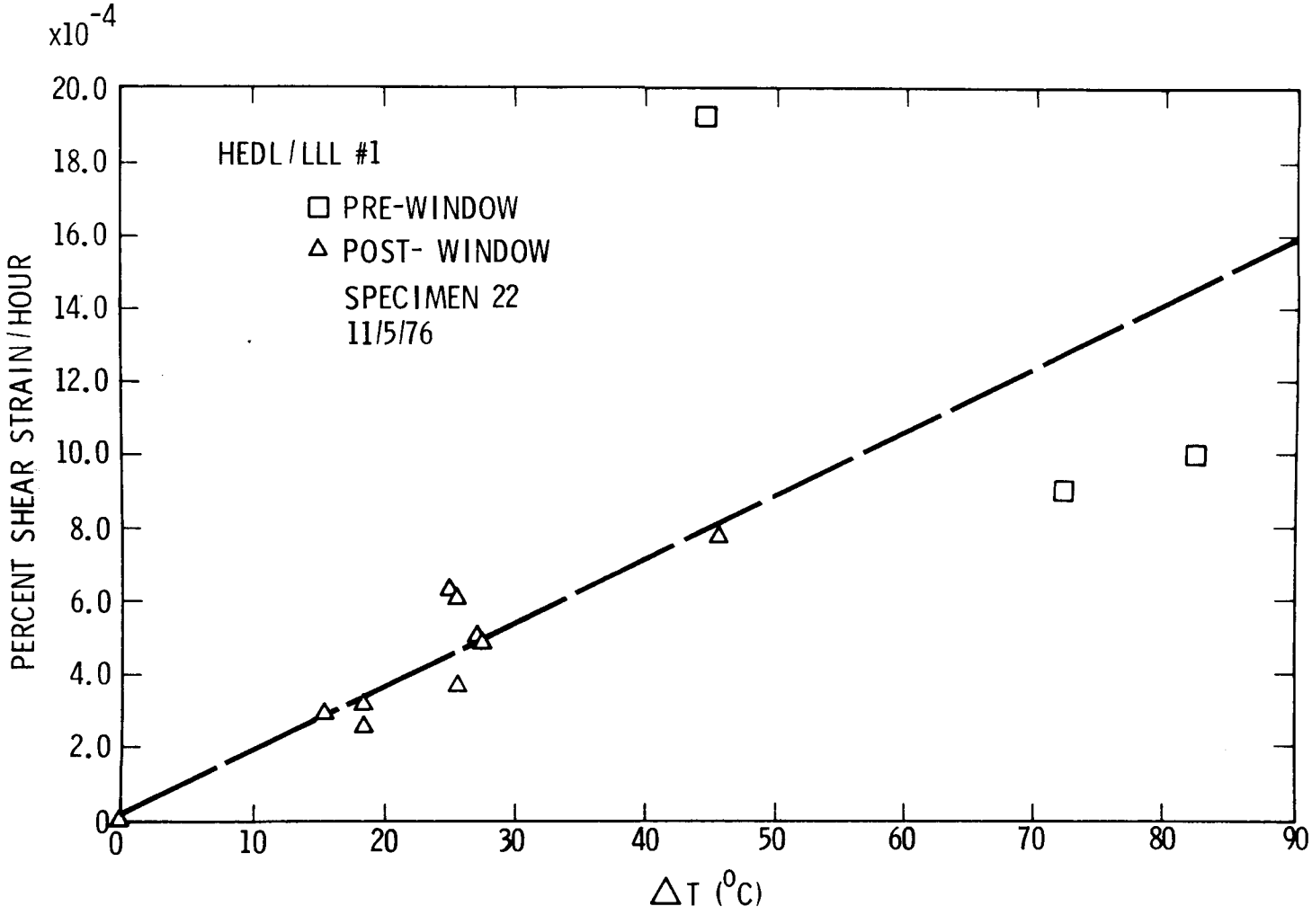

FIGURE 9. Creep Rates Versus Proton Flux Density.

HEDL 7611-110.4

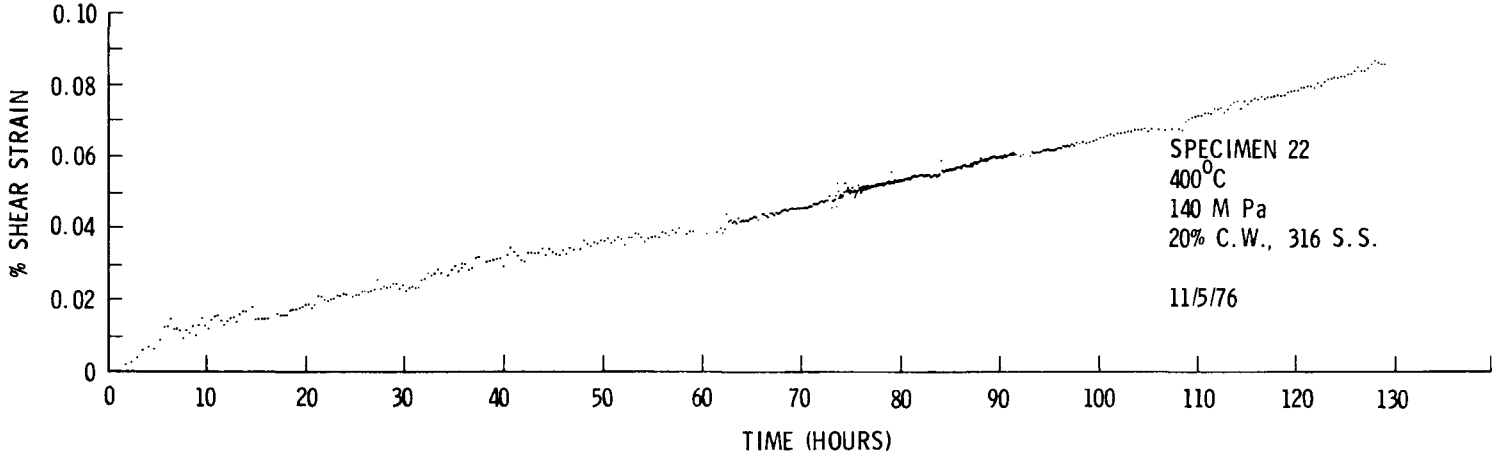

HEDL 7611-110.1

FIGURE 10. Irradiation Creep as a Function of Dose or Time. Approximate Displacement Rate is $4(^{+3}_{-1}) \times 10^{-7}$/sec.

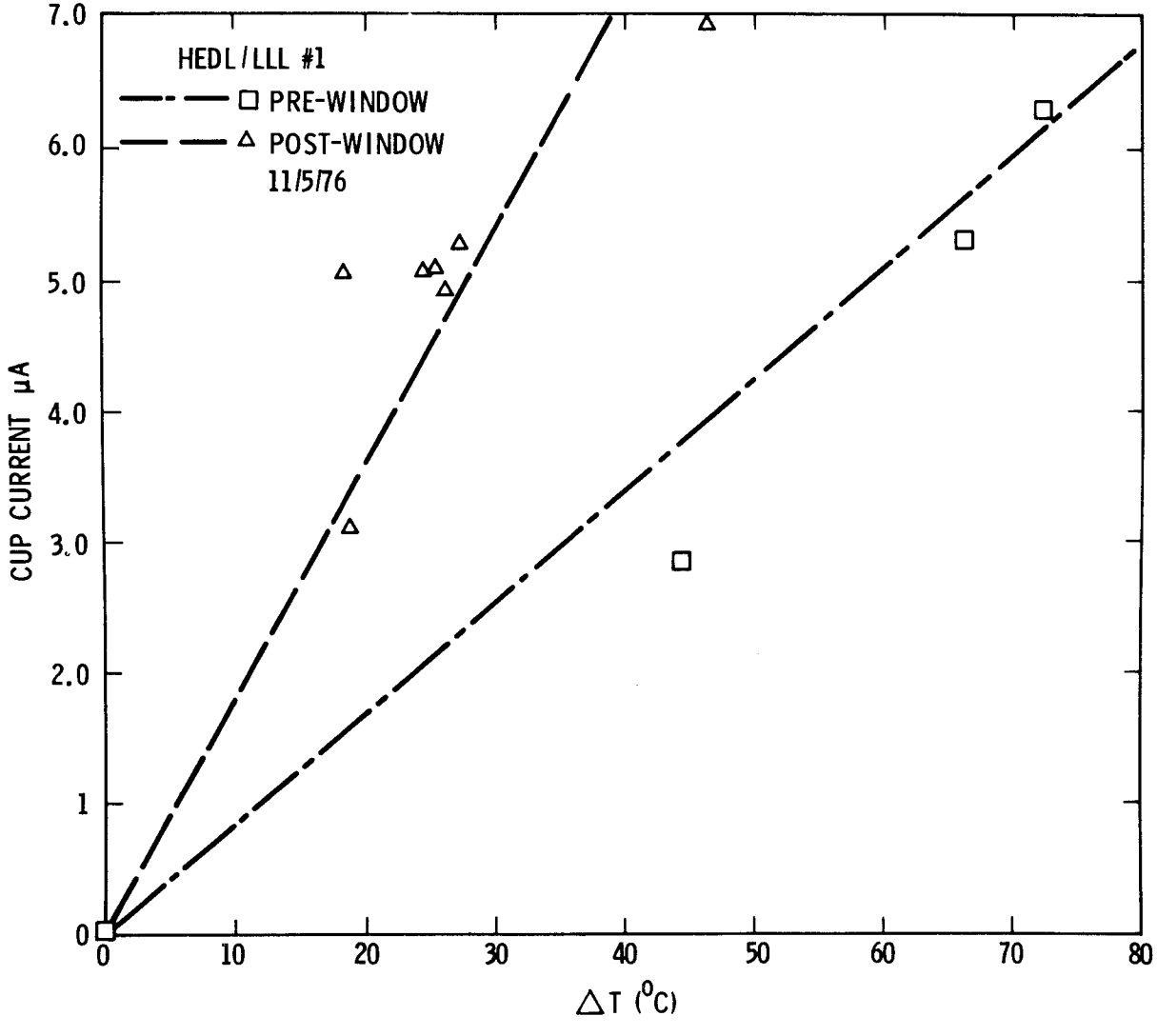

FIGURE 11. Relationship Between the Two Fundamental Measures of Beam Density. HEDL 7611-110.6

PREPARATION AND PRESENTATION OF DESIGN DATA (ED-02-03 EDC)

PREPARATION AND PRESENTATION OF DESIGN DATA

M. F. Marchbanks, R. A. Moen and J. C. Spanner (HEDL)

I. OBJECTIVE

The objective of this program is to provide an authoritative source of materials design data for common use throughout the national Magnetic Fusion Energy (MFE) Program. The data will be incorporated into the existing Nuclear Systems Materials Handbook, TID-26666, and provided to designated MFE Program participants.

II. SUMMARY

The overall scope of the Nuclear Systems Materials Handbook has been expanded to address the needs of current and future MFE projects. Copies of the Handbook have been provided to all organizations now participating in near term MFE projects.

III. ACCOMPLISHMENTS AND STATUS

- Dr. E. N. C. Dalder from ERDA's Division of Magnetic Fusion Energy has become an official member of the Advisory Group, joining 18 others in guiding the overall Nuclear Systems Materials Handbook program.

- Twelve additional sets of the Handbook were provided to MFE contractor organizations. Handbooks at ORNL, HEDL, BNW, LASL, GA and Westinghouse are being used for MFE work, in addition to their use on other advanced nuclear energy systems.

- Update packages containing 175 new and revised pages were distributed to all Handbook users during the reporting period.

IV. EXPECTED ACCOMPLISHMENTS

- Concerted efforts will be started to document materials data requirements for the near term MFE projects. These will become part of a total matrix of advanced nuclear energy systems materials requirements.

- Approximately 200 additional pages will be prepared and distributed within the MFE community on materials/properties of mutual interest to a number of advanced nuclear energy systems.

V. COMMUNICATIONS AND MEETINGS

The Advisory Group met at Atomics International on November 4-5, 1976. Minutes for that meeting were transmitted by J. C. Spanner to all Advisory Group members on November 24, 1976.

VI. REPORTS AND PUBLICATIONS

- Update Package No. 4 - transmittal letter dated 10/4/76.

- Update Package No. 5 - transmittal letter dated 11/11/76.

DISTRIBUTION FOR MFE QUARTERLY REPORTS

UC-20 (190)

APPROVED SPECIAL DISTRIBUTION (126)

Argonne National Laboratory (13)

9700 South Cass Avenue
Argonne, Illinois 60439
- Director, ANL MFE Program (2)
- Director, Materials Science Division
- D. M. Gruen
- S. D. Harkness
- R. Heinrich
- M. S. Kaminsky
- R. J. Kennerly
- V. H. Maroni
- F. V. Nolfi
- P. J. Persiani
- A. Taylor
- H. Wiedersich

Atomics International (4)

Component Engineering and Technology Division
North American Rockwell
8900 De Soto Avenue
Canoga Park, California 91304
- Manager, Materials and Physics Technology
- H. Farrar IV
- D. Kramer
- D. W. Keefer

Brookhaven National Laboratory (4)

Associated Universities
Upton, New York 11973
- Chairman, Department of Applied Sciences (2)
- Associate Chairman for Chemistry and Materials Programs, Department of Applied Sciences
- A. N. Goland

University of California - Santa Barbara (2)

Department of Chemical and Nuclear Engineering
Santa Barbara, California 93106
- G. R. Odette (2)

University of Cincinnati (1)

Department of Materials Sciences and Metallurgical Engineering
216 Basic Science Building
Cincinnati, Ohio 45221
J. Moteff

Columbia University (2)

Plasma Physics Laboratory
New York, New York 10027
R. A. Gross
R. J. Tien

Cornell University (1)

Ithaca, New York 14850
C. Y. Li

Electric Power Research Institute (1)

3412 Hillview Avenue
Palo Alto, California 94304
Program Manager for Fusion Power

Energy Research and Development Administration (21)

Washington, D. C. 20545
Assistant Director for Materials Sciences Program, DPR (2)
Assistant Director for Technology, RDD
Chief, Fuel Systems Branch, RDD
Chief, Materials and Chemistry Branch, Office of Technology, RDD
Assistant Director, D&T, DMFE
Chief, Systems Studies and Applications Branch, D&T, MFE
Chief, Materials and Radiation Effects Branch, MFE (4)
Assistant Director for Confinement Systems, MFE
Assistant Director for Plasma Physics, MFE
Assistant Director for Technical Projects
Director, MFE Division
N. A. Davies
J. F. Decker
P. B. Hemmig
K. G. Moses
R. E. Price
F. T. Scott

DISTRIBUTION FOR MFE QUARTERLY REPORTS (Cont'd)

General Atomic Company (4)

P.O. Box 81608
San Diego, California 92138
Manager, Fusion Engineering Department
C. Baker
G. R. Hopkins
L. Rovner

Grumman Aerospace Corporation (2)

Materials and Process Department
Bethpage, New York 11714
Chief, Materials and Process Department
Chief, Nuclear Physics Research Department

Jersey Nuclear Company (1)

777 106th Avenue, N.E.
Bellevue, Washington 98004
H. K. Forsen

Lawrence Livermore Laboratory (7)

University of California
P. O. Box 808
Livermore, California 94550
Director, CTR Division
Director, E Division
Program Manager for CTR, Chemistry and Materials Sciences Dept. (2)
J. Davis
M. W. Guinan
C. M. Logan

Los Alamos Scientific Laboratory (8)

University of California
P.O. Box 1663
Los Alamos, New Mexico 87544
Division Leader, CTR Division
Division Leader, CMB Division
Division Leader, P Division
F. W. Clinard
D. J. Dudziak
C. R. Emigh
W. Green
D. M. Parkin

McDonnell-Douglas Astronautics (1)

P.O. Box 516
St. Louis, Missouri 63166
D. Kummer

Massachusetts Institute of Technology (3)

Cambridge, Massachusetts 02139
L. Lidsky, Dept. of Nuclear Engineering
K. Russell, Dept. of Materials Science
O. Harling, Nuclear Reactor Laboratory

University of Michigan (1)

Nuclear Engineering Department
College of Engineering
Ann Arbor, Michigan 48105
T. Kammash

Mound Laboratory (1)

P.O. Box 32
Miamisburg, Ohio 45342
Manager, Technology Applications and Development

National Bureau of Standards (1)

Room C-225
Washington, D. C. 20234
Director, Center for Radiation Research

Naval Research Laboratory (3)

Metallurgy Division, Code 6390
Washington, D. C. 20375
Head, Thermo Structural Materials Branch
I. Manning
F. A. Smidt

North Carolina State University (2)

Department of Nuclear Engineering
Raleigh, North Carolina 26707
J. R. Beeler, Jr.
T. S. Elleman

Oak Ridge National Laboratory (16)

P.O. Box Y
Oak Ridge, Tennessee 37830
- Director, Thermonuclear Division, Bldg. 9201-2
- Director, Metals and Ceramics Division
- Program Manager, Fusion Reactor Technology Program, Bldg. 9204-1
- Manager, Controlled Thermonuclear Reactor Materials, Metals and Ceramics Division, Bldg. 4500S
- B. R. Appleton
- C. R. Brinkman
- R. J. Colchin, Bldg. 9201-2
- J. H. Devan, Bldg. 4500S
- J. A. Horak, Bldg. 4500S
- W. R. Martin, Bldg. 4500S
- F. G. Perey
- M. Roberts, Bldg. 9204-1
- M. T. Robinson
- J. O. Stiegler
- C. Weisbin
- F. W. Wiffen, Bldg. 4500S

Ohio State University (1)

1659 N. High
Columbus, Ohio 43210
- P. Shewmon, Dept. of Metallurgy

Pacific Northwest Laboratory (8)

Battelle Memorial Institute
P.O. Box 999
Richland, Washington 99352
- Manager, Fusion Programs
- J. L. Brimhall
- T. Chikalla
- A. B. Johnson
- R. Jones
- R. P. Marshall
- L. C. Schmid
- D. Styris

Plasma Physics Laboratory (6)

Princeton University
Forrestal Campus
Box 451
Princeton, New Jersey 08540
Director, Plasma Physics Laboratory
Project Manager, TFTR
S. Cohen
C. Osgood
W. Price
K. Wakefield

Sandia Laboratories (2)

Albuquerque, New Mexico 87115
F. L. Vook (2)

Sandia Laboratories (2)

Livermore, California 94550
W. Bauer (2)

University of Virginia (1)

Department of Materials Science
Research Labs for Engineering Sciences
Charlottesville, Virginia 22901
H. G. F. Wilsdorf

Westinghouse Electric Company (1)

Nuclear Center
P.O. Box 355
Pittsburgh, Pennsylvania 15230
Manager, Fusion Power Systems Department

Westinghouse Electric Corporation (3)

Research and Development Center
Beulah Road
Pittsburgh, Pennsylvania 15234
R. Gold
H. R. Holland
R. Begley

University of Wisconsin-Madison (2)

Department of Nuclear Engineering
Madison, Wisconsin 53706
Gerald L. Kulcinski (2)

University of Wisconsin-Milwaukee (1)

Department of Physics
Milwaukee, Wisconsin 53201
D. Lichtmann

INTERNAL DISTRIBUTION FOR MFE QUARTERLY REPORTS

Hanford Engineering Development Laboratory (38)

T. K. Bierlein
H. R. Brager
M. C. J. Carlson
T. T. Claudson
D. G. Doran (2)
E. A. Evans
F. A. Garner
R. Gold
B. R. Hayward
J. J. Holmes
J. E. Irvin
R. L. Knecht
M. K. Korenko
J. J. Laidler
E. P. Lippincott
W. M. McElroy
J. W. Niestlie
R. E. Nygren
E. K. Opperman
W. E. Roake
J. O. Schiffgens
W. F. Sheely
R. L. Simons
J. C. Spanner
A. Squire
J. L. Straalsund
G. L. Wire
H. H. Yoshikawa
Central Records and Files (8)
Publication Services (1)

ERDA-RL (5)

Manager
Assistant Manager for Technical Operations
Chief Patent Attorney
Chief, Energy Programs Division
W. A. Burns, Program Engineer, Energy Programs Divison